Gastroenterology 2022;162:1242–1255

BASIC AND TRANSLATIONAL—PANCREAS

Docking Protein p130Cas Regulates Acinar to Ductal Metaplasia During Pancreatic Adenocarcinoma Development and Pancreatitis

Andrea Costamagna,[1,*] **Dora Natalini**,[1,*] Maria del Pilar Camacho Leal,[1] Matilde Simoni,[2] Luca Gozzelino,[1] Paola Cappello,[1,3] Francesco Novelli,[1,3] Chiara Ambrogio,[1] Paola Defilippi,[1] Emilia Turco,[1] Elisa Giovannetti,[4,5] Emilio Hirsch,[1] Sara Cabodi,[1,§] and Miriam Martini[1,§]

[1]Molecular Biotechnology Center, Department of Molecular Biotechnology and Health Sciences, University of Torino, Turin, Italy; [2]IRCCS Ospedale San Raffaele, Preclinical Models of Cancer Unit, Milan, Italy; [3]Laboratory of Tumor Immunology, Center for Experimental Research and Medical Studies, Città della Salute e della Scienza di Torino, University of Torino, Torino, Italy; [4]Cancer Pharmacology Laboratory, AIRC-Start-Up, Fondazione Pisana per la Scienza, San Giuliano Terme, Pisa, Italy; and [5]Department of Medical Oncology, Cancer Center Amsterdam, Amsterdam University Medical Centers, Vrije Universiteit, Amsterdam, The Netherlands

See editorial on page 1037.

BACKGROUND & AIMS: Acinar to ductal metaplasia is the prerequisite for the initiation of Kras-driven pancreatic ductal adenocarcinoma (PDAC), and candidate genes regulating this process are emerging from genome-wide association studies. The adaptor protein p130Cas emerged as a potential PDAC susceptibility gene and a Kras-synthetic lethal interactor in pancreatic cell lines; however, its role in PDAC development has remained largely unknown. **METHODS:** Human PDAC samples and murine $Kras^{G12D}$-dependent pancreatic cancer models of increasing aggressiveness were used. p130Cas was conditionally ablated in pancreatic cancer models to investigate its role during Kras-induced tumorigenesis. **RESULTS:** We found that high expression of p130Cas is frequently detected in PDAC and correlates with higher histologic grade and poor prognosis. In a model of Kras-driven PDAC, loss of p130Cas inhibits tumor development and potently extends median survival. Deletion of p130Cas suppresses acinar-derived tumorigenesis and progression by means of repressing PI3K–AKT signaling, even in the presence of a worsening condition like pancreatitis. **CONCLUSIONS:** Our observations finally demonstrated that p130Cas acts downstream of Kras to boost the PI3K activity required for acinar to ductal metaplasia and subsequent tumor initiation. This demonstrates an unexpected driving role of p130Cas downstream of Kras through PI3K/AKT, thus indicating a rational therapeutic strategy of targeting the PI3K pathway in tumors with high expression of p130Cas.

Keywords: ADM; Kras; Metaplasia; Carcinogenesis; PDAC.

Pancreatic ductal adenocarcinoma (PDAC) is on path to become the second leading cause of cancer-related death by 2030, as this remains one of the most lethal oncologic conditions worldwide, regardless of more effective combination treatments and new diagnostic possibilities.[1,2]

The first genetic event on the road to invasive pancreatic cancer is mutational activation of Kras, which occurs in the earliest precancerous lesions.[3,4] Because the direct targeting of Kras is difficult, understanding the processes that lead to pancreatic cancer initiation is crucial both for the identification of early detection markers and for the development of early intervention modalities. Despite the ductal characteristics of this cancer, studies in mouse models of Kras-driven tumors indicate that PDAC can arise from acinar cells that undergo a transdifferentiation event, termed *acinar to ductal metaplasia* (ADM).[5–7] Acinar cells show a high degree of plasticity and readily de-differentiate to ductal-like intermediates in response to Kras activity. Conversely, ductal cells require additional mutations in classical tumor suppressor genes, such as TP53, SMAD4, or BRCA1, to be efficiently transformed by Kras.[8–11]

Genes that specifically control this plasticity and explain why the 2 cell types behave differently are largely unknown, but candidate genes, like the Nr5a2 orphan hormone nuclear receptor that inhibits Kras-driven ADM,[12,13] are emerging from genome-wide association studies. Among the few other genes identified in these genome-wide association studies, BCAR1 (breast cancer anti-estrogen resistance 1) emerges as a potential pancreatic cancer susceptibility gene.[14–16]

The BCAR1 gene encodes for the p130Cas adaptor protein, a nodal platform on which integrin and growth factor receptor signaling converge to promote oncogenic transformation of various cell types.[17–20] In pancreatic cancer cell lines, p130Cas has emerged as a Kras-synthetic lethal interactor, sensitizing pancreatic tumors to ERK inhibition

*Authors share co-first authorship; §Authors share co-senior authorship.

Abbreviations used in this paper: ADM, acinar to ductal metaplasia; CK19, cytokeratin 19; 3D, 3-dimensional; PanIN, pancreatic intraepithelial neoplasia; PDAC, pancreatic ductal adenocarcinoma; WT, wild-type.

Most current article

0016-5085
https://doi.org/10.1053/j.gastro.2021.12.242

WHAT YOU NEED TO KNOW

BACKGROUND AND CONTEXT

Development of pancreatic ductal adenocarcinoma (PDAC) involves Kras-induced acinar to ductal metaplasia, which requires full activation of the PI3K–AKT signaling pathway.

NEW FINDINGS

We discovered that p130Cas adaptor protein mediates the activation of PI3K that is indispensable for oncogenic Kras-driven acinar to ductal metaplasia. Phosphorylated p130Cas binds to p85α PI3K-regulatory subunit and allows full activation of PI3K catalytic activity downstream mutant Kras and EGFR. High p130Cas levels support initial pancreatic tumorigenesis and associate with significantly worsen patient survival.

LIMITATIONS

The adaptor p130Cas represents a point of convergence between integrin and RTK signaling pathways. The 3-dimenstional culture model used in this article, although more physiological than 2-dimensional culture, could be improved to understand the relative contribution of these signaling pathways to PDAC initiation.

IMPACT

The role of p130Cas as a key player in acinar to ductal metaplasia underscores the importance of PI3K–AKT regulators in PDAC initiation.

via Myc regulation[21]; however, its role in PDAC development has remained largely unknown.

In the present study, we genetically deleted p130Cas in murine pancreatic cancer models of increasing aggressiveness to investigate the role of p130Cas during Kras-induced tumorigenesis. We found that pancreatic deletion of murine p130Cas abrogates Kras-dependent ADM and potently improved survival. In agreement with these results, patients stratified with lower p130Cas expression presented a significantly extended lifespan. Our observations finally demonstrated that p130Cas acts downstream of Kras to boost the PI3K activity required for ADM and subsequent tumor initiation, thus indicating an unsuspected pathway crucial for Kras-driven PDAC.

Methods

The methods are detailed in the Supplementary Material.

Results

p130Cas Is Overexpressed During Pancreatic Ductal Adenocarcinoma Onset and Independently Predicts Poor Patient Prognosis

To validate the association between p130Cas and pancreatic cancer susceptibility, we selected a cohort of early-stage patients (stage I–IIb, n = 98) and examined p130Cas expression by immunohistochemistry. Low levels of p130Cas were found in approximately 40% of the patients, and approximately 60% of the patients were classified as high expressors (Figure 1*A*). Notably, analysis of publicly available datasets of pancreatic cancer (GSE16515, GSE62452, and GSE28735)[22–24] also displayed elevated p130Cas messenger RNA in pancreatic tumors compared with normal tissue (Supplementary Figure 1*A*). Correlation with overall survival and progression-free survival was evaluated with Kaplan–Meier curves and the log-rank test. Univariate analysis was performed and factors with a P value $<.1$ were evaluated in the multivariate analysis using the backward stepwise elimination (Wald) method, as described previously.[25] Remarkably, patients with high p130Cas expression experienced significantly shorter overall survival and progression-free survival (Figure 1*B* and *C*). In addition, we found that p130Cas expression remained an independent predictor of survival, even after stratification for tumor grading and vascular infiltration in multivariate analysis (Table 1). Taken together, these data suggested that high p130Cas levels support initial pancreatic tumorigenesis and associate with significantly worsen patient survival.

p130Cas Is Critical for the Initiation of Preneoplastic Acinar to Ductal Metaplasia Lesions by Kras and Tissue Injury

We took advantage of Pdx^{Cre}; $Kras^{G12D}$ and Pdx^{Cre}; $Kras^{G12D}$; $Trp53^{R172H}$ pancreatic cancer mouse models (referred to hereinafter as $Kras^{G12D}$ and $Kras^{G12D}$; $Trp53^{R172H}$)[26,27] to investigate the role of p130Cas during Kras-dependent pancreatic tumorigenesis. Of note, p130Cas expression was very low or undetectable in normal pancreatic acini and normal ducts (Figure 2*A, left panel*). Similar to what was observed in patients, p130Cas was overexpressed in high-grade lesions in both murine models. Specifically, p130Cas staining intensity was increased, even if heterogeneously, in low-grade ADM and pancreatic intraepithelial neoplasia (PanIN)1–2 lesions of 2- and 4-month-old $Kras^{G12D}$ mice (Figure 2*A, central panels*), as well as in high-grade PanIN3 lesions and PDAC areas of $Kras^{G12D}$; $Trp53^{R172H}$ mice (Figure 2*A, right panel*), but remained low or undetectable in the adjacent stroma and immune cells. As shown in Figure 2*B* and *C*, p130Cas expression did not increase further from ADM to PDAC lesions, but the areas with high p130Cas expression increased in parallel to tumor progression.

Because p130Cas expression increased in early ADM lesions, we employed an additional in vivo model to understand its regulation. Pancreatic damage and pancreatitis force acinar cells to undergo the metaplastic transition, exacerbating the formation of ADM lesions by mutated Kras.[28,29] To assess whether p130Cas expression levels were regulated during ADM, control (Pdx^{Cre}; $Kras^{wt/wt}$) and $Kras^{G12D}$ mice were treated with caerulein, a known pancreatitis inducer (see Methods section in the Supplementary Material; Supplementary Figure 1*B*). As shown in Figure 2*D–F*, after 1 day of caerulein treatment, p130Cas expression increased in acinar cells undergoing ADM, regardless of the Kras status. In the absence of oncogenic Kras, redifferentiation into functional acinar cells occurred within 1 week, together with the

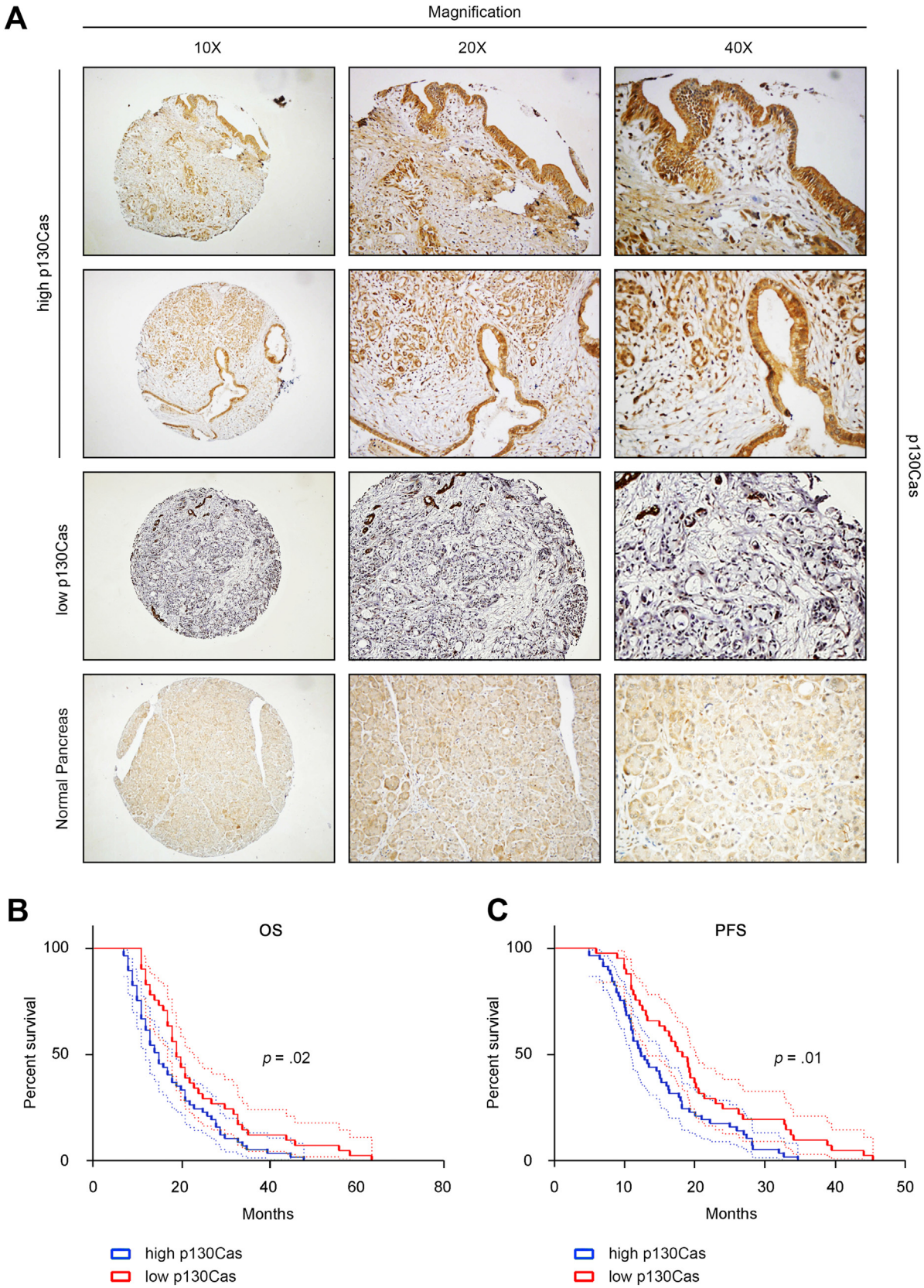

Figure 1. p130Cas is overexpressed during PDAC onset and independently predicts poor patient prognosis. (*A*) Representative results from immunohistochemical staining of p130Cas in human PDAC (n = 98) and normal pancreas (n = 4) samples. (*B, C*) Kaplan–Meier curves showing significantly lower overall survival (*left panel*) and progression-free survival (*right panel*) in patients with elevated p130Cas staining (*blue*) than with low p130Cas staining (*red*). Statistical analysis was performed with Mantel–Cox log-rank test.

Table 1. Patients' Clinicopathologic Characteristics and Outcomes

	Overall survival			Progression-free survival		
Univariate analysis	n (%)	Months, mean (95% CI)	*P* value	n (%)	Months, mean (95% CI)	*P* value
No. patients	98 (100)	20.5 (18.2–22.8)	—	98 (100)	17.3 (15.5–19.1)	
Age at time of diagnosis			.352			.224
65 y or younger	60 (61.2)	21.28 (16.4–22.1)		60 (61.2)	18.9 (15.6–20.5)	
Older than 65 y	38 (38.8)	19.26 (17.9–24.6)		38 (38.8)	16.2 (13.7–18.6)	
Sex			.081			.686
Female	41 (41.8)	23.0 (19.0–27.1)		41 (41.8)	17.9 (15.2–20.7)	
Male	57 (58.2)	18.7 (15.9–21.4)		57 (58.2)	16.9 (14.5–19.2)	
Performance status			.200			.154
0–1	77 (78.6)	21.2 (18.5–24.0)		77 (78.6)	17.9 (15.8–20.0)	
2	21 (21.4)	17.8 (13.8–21.9)		21 (21.4)	15.4 (12.2–18.5)	
Vascular infiltration			.011			.019
No	36 (36.7)	24.6 (20.2–29.0)		36 (36.7)	20.1 (16.9–23.5)	
Yes	62 (63.3)	18.1 (15.6–20.6)		62 (63.3)	15.7 (13.7–17.6)	
Tumor grade			.035			.027
1–2	49 (50.0)	22.9 (19.2–26.7)		49 (50.0)	19.7 (16.9–22.4)	
3	49 (50.5)	18.1 (15.4-20.7)		49 (50.5)	15.0 (12.8–17.1)	
Resection margin			.220			.198
No	52 (53.1)	18.8 (15.3–22.4)		52 (53.1)	18.5 (15.9–20.9)	
Yes	46 (46.9)	21.9 (18.6–24.7)		46 (46.9)	16.1 (13.5–18.6)	
p130Cas/BCAR1			.017			.005
Low	41 (41.8)	23.9 (19.8–28.2)		41 (41.8)	20.3 (17.1–23.3)	
High	57 (58.2)	18 (15.5–20.6)		57 (58.2)	15.2 (13.2–17.2)	

Multivariate analysis	Risk of death, HR (95% CI)	*P* value	Risk of progression, HR (95% CI)	*P* value
Vascular infiltration (no vs yes)	0.47 (0.22–0.81)	.033	0.58 (0.28–0.79)	.038
Grading (3 vs 1–2)	0.62 (0.29–0.95)	.047	0.61 (0.30–0.87)	.042
p130Cas/BCAR1 (low vs high)	0.51 (0.25–0.87)	.044	0.34 (0.21–0.72)	.031

HR, hazard ratio.

reduction of p130Cas expression, suggesting that p130Cas was up-regulated during ADM but returned minimal during pancreatic repair (Figure 2*D*–*F*). Conversely, $Kras^{G12D}$ mice displayed persistent p130Cas up-regulation in metaplastic acini and in subsequent PanIN lesions. In agreement, p130Cas messenger RNA levels detected in publicly available datasets (GSE41418, GSE109227, and GSE77983)[30–32] of caerulein-induced pancreatitis in wild-type (WT) and $Kras^{G12D}$ mice were significantly up-regulated (Supplementary Figure 1*C*).

These data suggest that p130Cas overexpression is critical for Kras-induced ADM and formation of preneoplastic lesions.

Cell Autonomous p130Cas Expression Is Critical for Acinar to Ductal Metaplasia

To assess whether p130Cas mediates ADM in a cell autonomous manner, we next adopted a physiological cell culture model of acinar to ductal transdifferentiation. Previous studies demonstrated that $Kras^{G12D}$ expression or EGFR stimulation induces the formation of ductal structures from acinar explants embedded in collagen[33,34] (Figure 3*A* and Supplementary Figure 1*D*). In isolated pancreatic acini, EGF treatment induced p130Cas phosphorylation in a dose-dependent manner (Supplementary Figure 1*E* and *F*). After 5 days, acini either treated with EGF or isolated from $Kras^{G12D}$ mice were able to transdifferentiate in vitro[34] and showed increased p130Cas phosphorylation and expression (Figure 3*B* and *C*) compared with control acini. Acini carrying the $Kras^{G12D}$ oncogene already displayed augmented p130Cas expression at day 1, and had the highest metaplastic potential in vitro (Figure 3*A* and Supplementary Figure 1*D*). Furthermore, ectopic p130Cas expression increased the formation of ductal structures from $Kras^{G12D}$ acini, while short hairpin RNA–mediated p130Cas down-modulation had the opposite effect (Figure 3*D* and *E* and Supplementary Figure 1*G* and *H*).

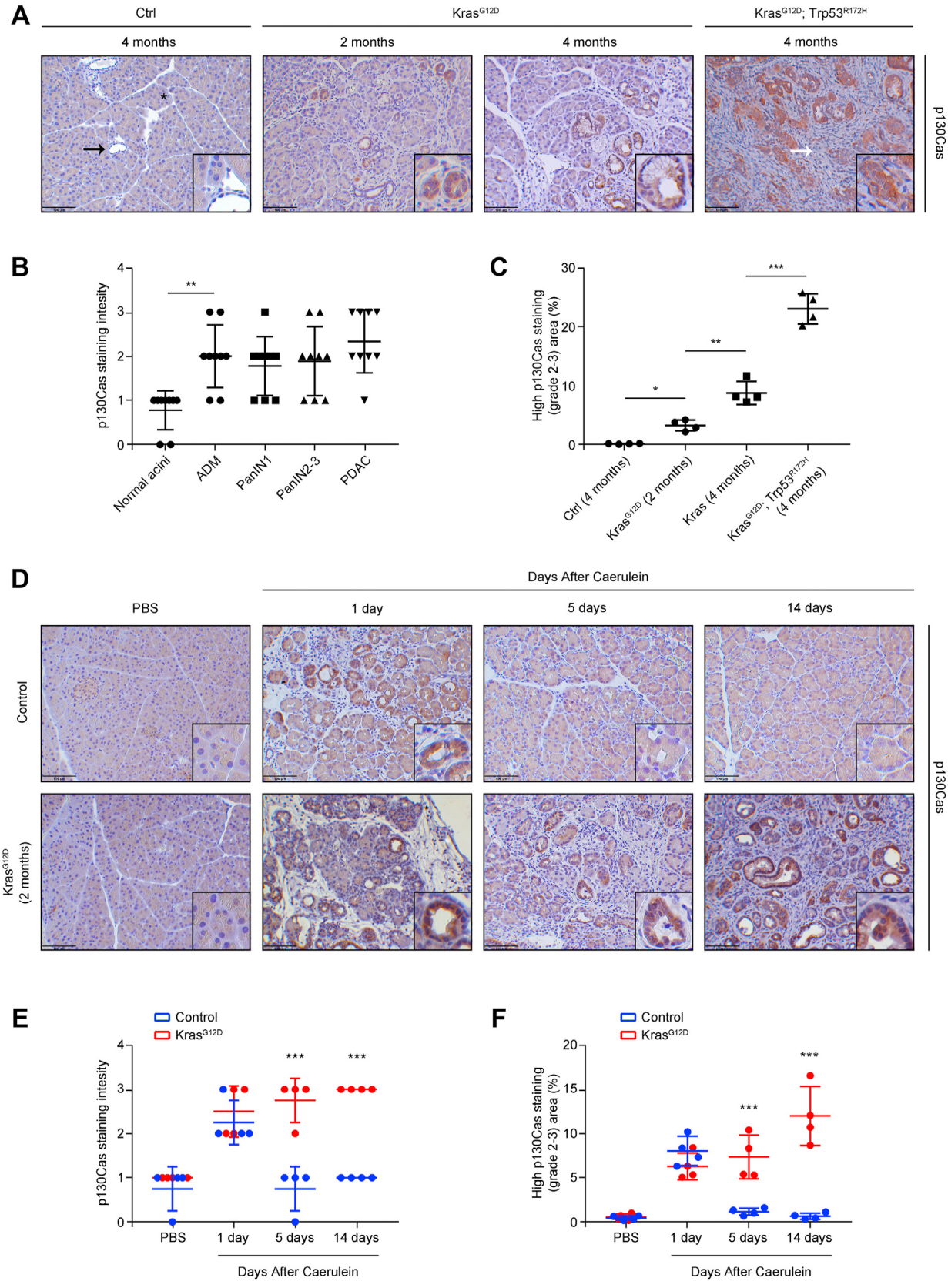
A
Ctrl
KrasG12D
KrasG12D; Trp53R172H
4 months
2 months
4 months
4 months
p130Cas
B
p130Cas staining intesity
Normal acini
ADM
PanIN1
PanIN2-3
PDAC
C
High p130Cas staining (grade 2-3) area (%)
Ctrl (4 months)
KrasG12D (2 months)
Kras (4 months)
KrasG12D; Trp53R172H (4 months)
D
Days After Caerulein
PBS
1 day
5 days
14 days
Control
KrasG12D (2 months)
p130Cas
E
Control
KrasG12D
p130Cas staining intesity
PBS
1 day
5 days
14 days
Days After Caerulein
F
Control
KrasG12D
High p130Cas staining (grade 2-3) area (%)
PBS
1 day
5 days
14 days
Days After Caerulein

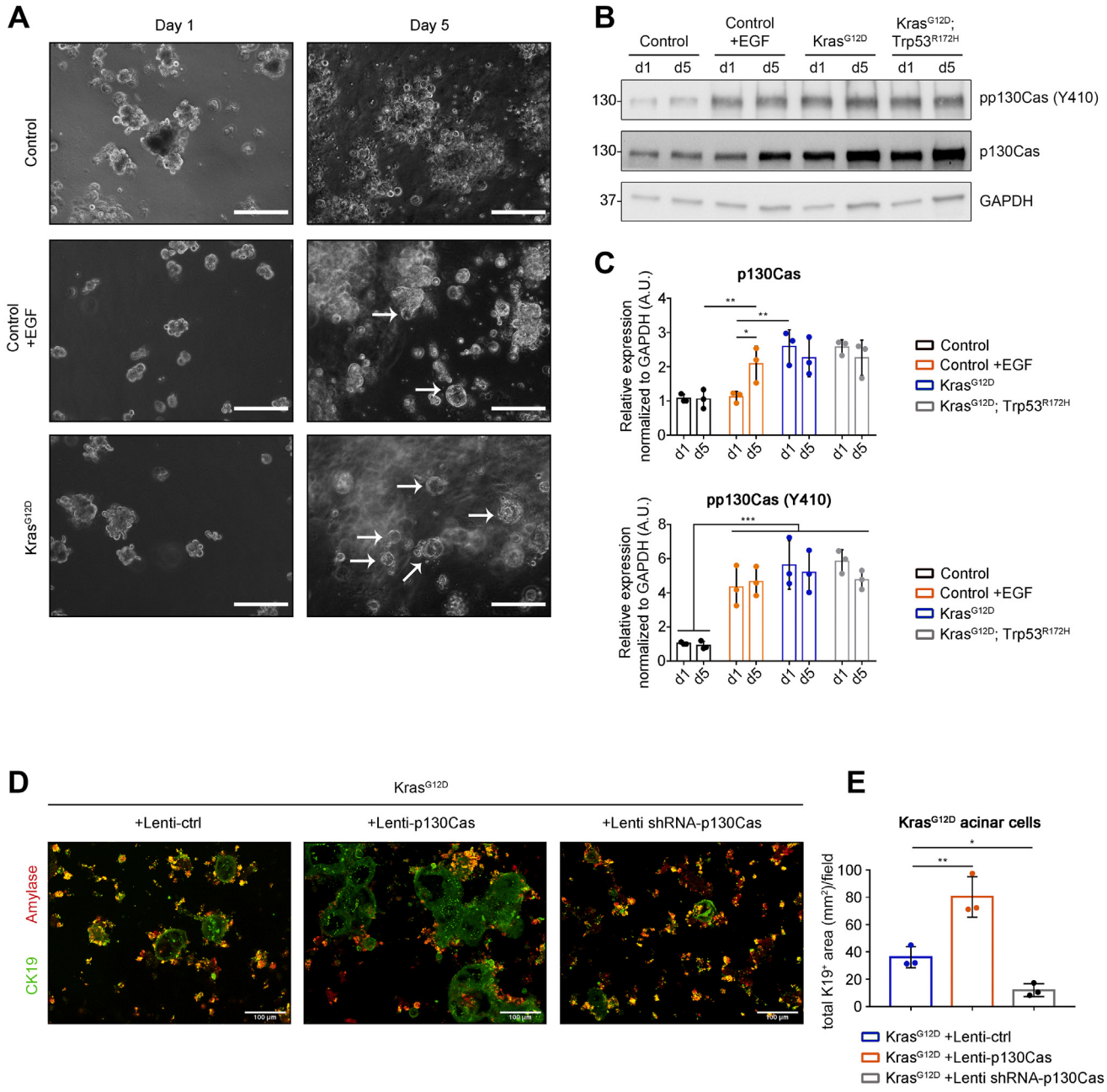

Figure 3. Cell autonomous p130Cas expression is critical for ADM. (*A*) Primary acinar cells were isolated from murine pancreata, seeded in 3D culture in collagen, and transdifferentiation was induced with EGF as indicated (quantification present in Supplementary Figure 1*D*). (*B, C*) Primary acinar cultures were subjected to Western blot to evaluate p130Cas phosphorylation (pp130Cas Y410) and expression, as indicated. Data reported are representative of at least 3 independent experiments. $^{**}P < .01$. (*D, E*) Primary acinar cells were transduced with lentiviral particles harboring ctrl, p130Cas, or short hairpin RNA against p130Cas and seeded as 3D culture. Immunofluorescent staining revealed amylase-positive acinar cells (*red*) or CK19-positive ductal structures (ADM) (*green*). The area stained by CK19 was quantified to score ADM formation. Statistical analyses were performed with 2-way analysis of variance. Data are presented as mean ± SD.

Figure 2. p130Cas is critical for the initiation of preneoplastic ADM lesions by Kras and tissue injury. (*A*) Immunohistochemical (IHC) staining for p130Cas in pancreatic tissue from control mice (Pdx^{Cre}; $Kras^{wt/wt}$), 2- and 4-month-old $Kras^{G12D}$ mice and 4-month-old $Kras^{G12D}$; $Trp53^{R172H}$ mice. *Asterisks* indicate normal pancreatic acinar tissue. *Black arrows* indicate normal pancreatic duct morphology. *White arrows* indicate stromal component. (*B*) Quantification of p130Cas IHC staining intensity, ranging from absent (0) to highest (3). (*C*) Quantification of the area with high (grade 2–3) p130Cas staining. (*D*) IHC for p130Cas in 2-month-old $Kras^{WT}$ (control, *upper panel*) and $Kras^{G12D}$ pancreata (*lower panel*) after phosphate-buffered saline or caerulein treatment. (*E*) Quantification of p130Cas immunohistochemical staining intensity, ranging from absent (0) to highest (3). (*F*) Quantification of the area with high (grade 2–3) p130Cas staining.

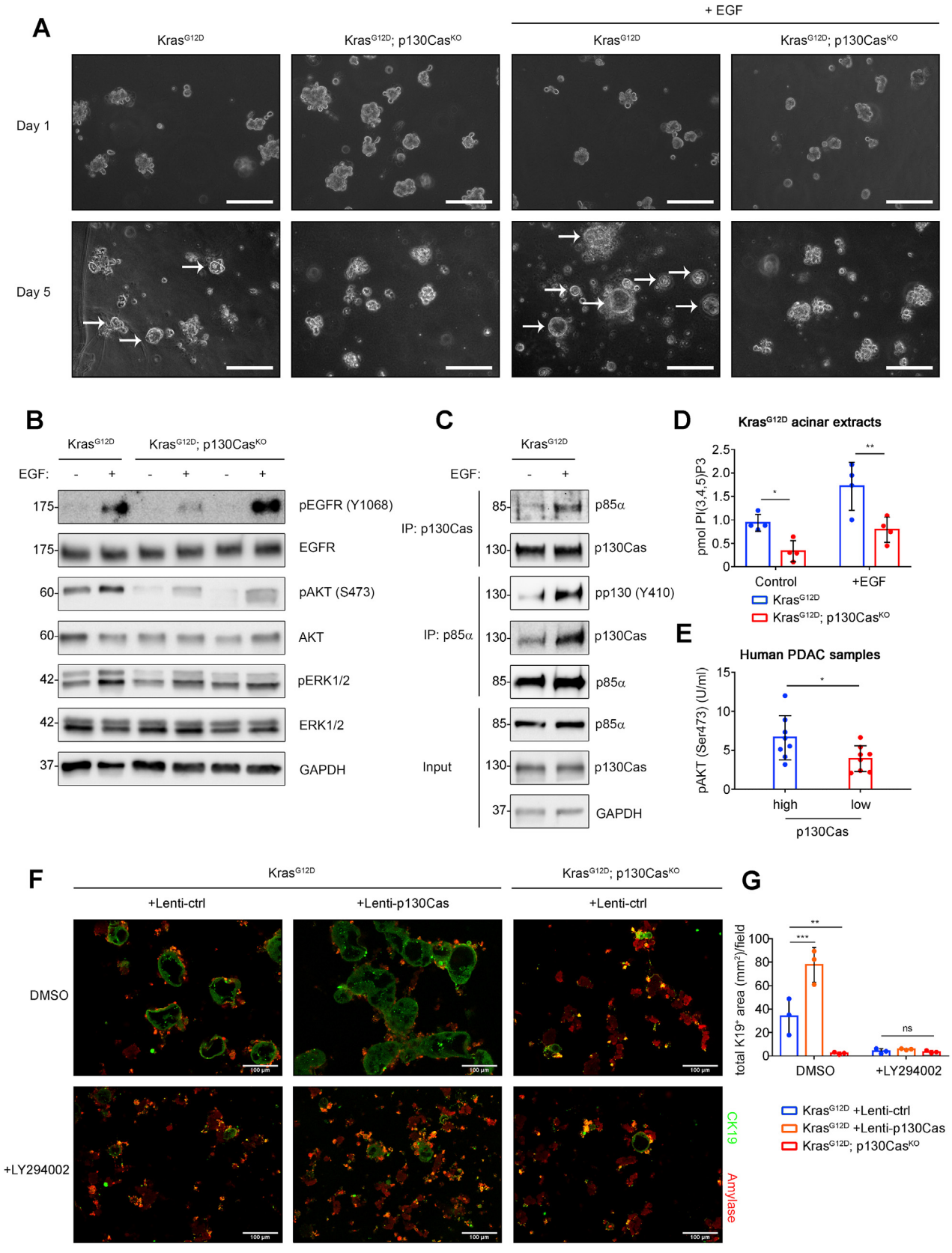
A
+ EGF
KrasG12D
KrasG12D; p130CasKO
KrasG12D
KrasG12D; p130CasKO
Day 1
Day 5
B
KrasG12D
KrasG12D; p130CasKO
EGF: - + - + - +
175- pEGFR (Y1068)
175- EGFR
60- pAKT (S473)
60- AKT
42- pERK1/2
42- ERK1/2
37- GAPDH
C
KrasG12D
EGF: - +
IP: p130Cas
85- p85α
130- p130Cas
IP: p85α
130- pp130 (Y410)
130- p130Cas
85- p85α
Input
85- p85α
130- p130Cas
37- GAPDH
D
KrasG12D acinar extracts
pmol PI(3,4,5)P3
Control
+EGF
KrasG12D
KrasG12D; p130CasKO
E
Human PDAC samples
pAKT (Ser473) (U/ml)
high
low
p130Cas
F
KrasG12D
KrasG12D; p130CasKO
+Lenti-ctrl
+Lenti-p130Cas
+Lenti-ctrl
DMSO
+LY294002
CK19
Amylase
G
total K19+ area (mm2)/field
DMSO
+LY294002
ns
KrasG12D +Lenti-ctrl
KrasG12D +Lenti-p130Cas
KrasG12D; p130CasKO

These data indicate that p130Cas expression levels are critical to mediate Kras-induced acinar metaplasia in a cell autonomous manner.

p130Cas Deletion Curbs Kras^{G12D}-Induced Acinar Metaplasia Ex Vivo

Overexpression of p130Cas during ADM suggested that loss of p130Cas could block Kras^{G12D}-driven acinar cell metaplasia. To test this hypothesis, we crossed Kras^{G12D} and Kras^{G12D}; Trp53^{R172H} models with mice carrying floxed p130Cas alleles (p130Cas$^{fl/fl}$)[35] to generate mice that specifically lack p130Cas expression in pancreatic epithelium (referred to hereinafter as Kras^{G12D}; p130Cas^{KO} and Kras^{G12D}; Trp53^{R172H}; p130Cas^{KO}). We employed a conditional approach to specifically delete p130Cas in the pancreatic epithelium and circumvent the embryonic lethality of germ-line p130Cas knockout.[36] To exclude gross pancreatic abnormalities in mice lacking p130Cas, pancreata from Pdx^{Cre}; p130Cas^{KO} mice were histologically examined. Both at birth and adulthood (4 months), these pancreata appeared normal, suggesting that p130Cas was dispensable for pancreas development (Supplementary Figure 2*A*). Suppression of p130Cas protein expression in pancreatic epithelium was confirmed by Western blot analysis (Supplementary Figure 2*B*). Pdx^{Cre}; p130Cas^{KO} mice were born at expected Mendelian ratio and were viable and fertile (Supplementary Figure 2*C*).

To assess whether p130Cas ablation was sufficient to block ADM in vitro, we explanted acini from Kras^{G12D} and Kras^{G12D}; p130Cas^{KO} mice and cultured them as 3-dimensional (3D) culture. As hypothesized, we observed significantly fewer ductal structures in Kras^{G12D}; p130Cas^{KO} acini than in Kras^{G12D}; p130Cas^{WT} controls (Figure 4*A* and Supplementary Figure 2*D*). Next, as EGF further increases the number of ductal structures from Kras^{G12D} explants,[37] we tested the extent of EGF-induced ADM in the presence or absence of p130Cas. Remarkably, EGF stimulation failed to sensitize Kras^{G12D}; p130Cas^{KO} acini to metaplastic transformation (Figure 4*A* and Supplementary Figure 2*D*). Similar results were obtained when ADM was induced with transforming growth factor–α (TGFα), an alternative EGFR ligand (Supplementary Figure 2*E* and *F*). These data indicate that loss of p130Cas blocks EGFR signaling to ADM in the presence of a hyperactive Kras^{G12D}.

p130Cas Ablation Suppresses Kras^{G12D}-Induced PI3K–AKT Signaling

Downstream of EGFR, p130Cas acts as a point of convergence between integrin and growth factor signaling and, therefore, its deletion could influence a variety of signaling pathways.[17,18] To establish which pathways were most affected by p130Cas during ADM, we analyzed 3D culture of primary acini isolated from Kras^{G12D} and Kras^{G12D}; p130Cas^{KO} mice by Western blot. We observed a moderate reduction of Myc protein in p130Cas^{KO} acini, but we did not score any difference in β-catenin activation or FAK (focal adhesion kinase) phosphorylation (Supplementary Figure 3*A* and *B*). This is in line with mouse genetics and pharmacology indicating that during ADM and pancreatic cancer development, one of the most critical signaling events is the activation of the PI3K/AKT pathway.[38–40] In agreement, Kras^{G12D} acini lacking p130Cas revealed a reduction in AKT phosphorylation both in basal condition and in the presence of EGF, with less evident effects on MEK1/2 and ERK1/2 phosphorylation (Figure 4*B* and Supplementary Figure 3*C* and *D*). This was not due to abnormal EGFR activation, as in the absence of p130Cas, EGF treatment efficiently promoted an increase in EGFR, AKT, MEK1/2, and ERK1/2 phosphorylation in acinar explants (Figure 4*B* and Supplementary Figure 3*C* and *D*).

In line with the view that p130Cas specifically amplifies targeted EGFR signaling, phosphorylated p130Cas directly binds to p85α PI3K-regulatory subunit, promoting PI3K activation.[41,42] We thus hypothesized that p130Cas may directly regulate PI3K activity in pancreatic acinar cells. To this end, we first tested p130Cas-p85α association in isolated Kras^{G12D} acini. In basal conditions, p85α was barely detectable in p130Cas immunoprecipitates, but p85α–p130Cas interaction increased after 10 minutes of EGF stimulation (Figure 4*C* and Supplementary Figure 3*E* and *F*). Moreover, we observed that p85α efficiently co-immunoprecipitated with tyrosine-phosphorylated p130Cas on EGF stimulation (Figure 4*C* and Supplementary Figure 3*E* and *F*). To confirm that p130Cas directly contributes to PI3K activation, we measured levels of PI(3,4,5)P3 in Kras^{G12D} acini and found that the loss of p130Cas significantly reduces the production of this lipid second messenger in basal conditions and, more strikingly, in the presence of EGF (Figure 4*D*). Accordingly,

Figure 4. p130Cas deletion curbs Kras^{G12D}-induced acinar metaplasia ex vivo and suppresses PI3K–AKT signaling. (*A*) Primary acinar cells were isolated from Kras^{G12D} and Kras^{G12D}; p130Cas^{KO} murine pancreata, seeded in 3D culture in collagen, and followed for spontaneous or EGF-induced transdifferentiation. Ducts (*arrows*) formed were photographed and counted. *Scale bar:* 100 μm. (*B*) Western blot (WB) of primary acinar cells isolated from murine pancreata and treated with phosphate-buffered saline (PBS) or EGF for 10 minutes, as indicated. (*C*) Primary acinar cells isolated from murine pancreata were treated with PBS or EGF for 10 minutes and subjected to immunoprecipitation with anti-p130Cas and anti-p85α antibodies. p130Cas/p85α interaction was revealed by WB with anti–phospho-p130Cas (pp130Cas Y410), anti-p130Cas, or anti-p85α antibodies as indicated. (*D*) Primary acinar cells isolated from murine pancreata were treated with PBS or EGF for 10 minutes and subjected to lipid extraction and PI(3,4,5)P3 enzyme-linked immunosorbent assay (ELISA). (*E*) Quantification of pAKT (Ser473) ELISA from high-p130cas (n = 8) and low-p130Cas (n = 8) human PDAC samples. (*F, G*) Primary acinar cells were transduced with lentiviral particles harboring ctrl or p130Cas, seeded in 3D culture, and pre-treated with dimethyl sulfoxide or LY294002 (10 μM) for 2 hours, as indicated. Immunofluorescent staining revealed amylase-positive acinar cells (*red*) or CK19-positive ductal structures (ADM) (*green*). Statistical analysis was performed with 2-way analysis of variance. *$P < .05$; **$P < .01$. Data are presented as mean ± SD.

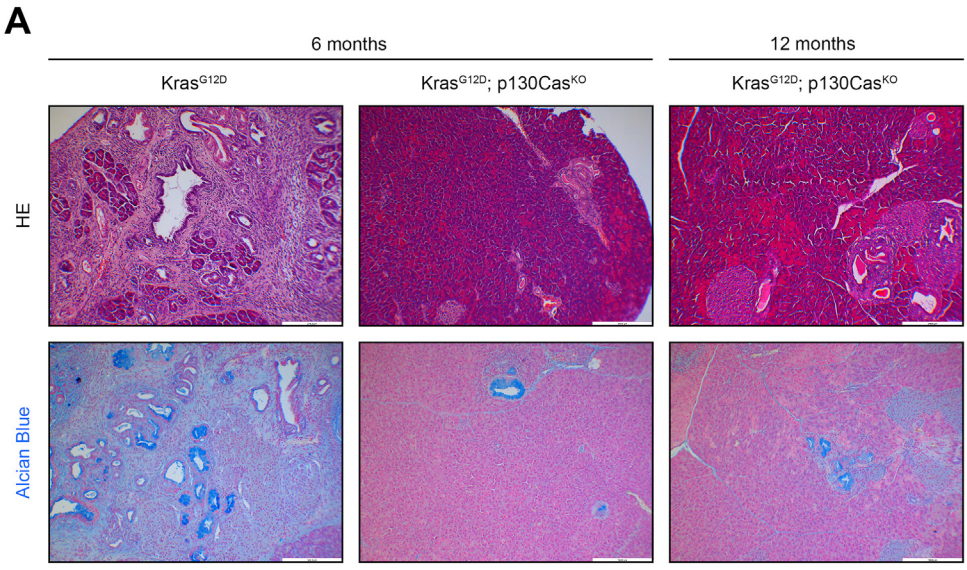
A
6 months
12 months
KrasG12D
KrasG12D; p130CasKO
KrasG12D; p130CasKO
HE
Alcian Blue

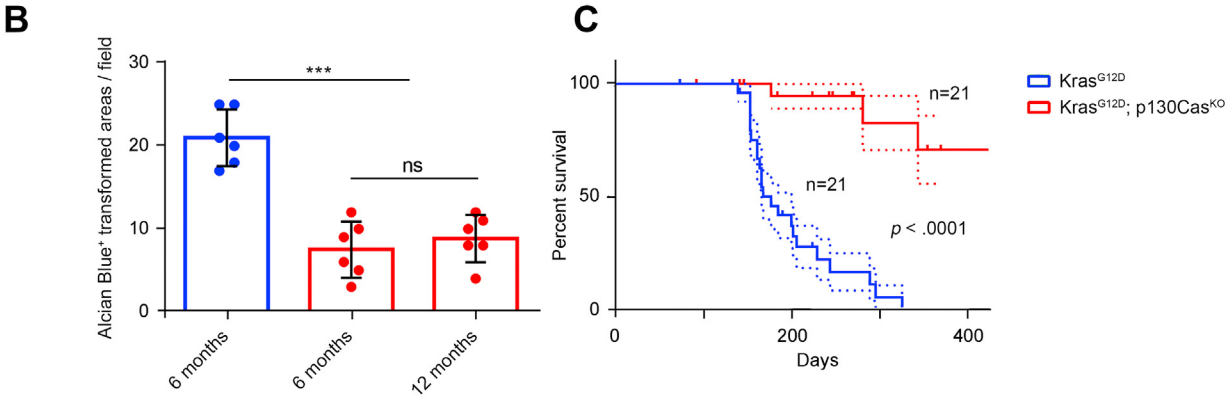
B
Alcian Blue+ transformed areas / field
30
20
10
0
***
ns
6 months
6 months
12 months
C
Percent survival
100
50
0
n=21
n=21
p < .0001
0
200
400
Days
KrasG12D
KrasG12D; p130CasKO

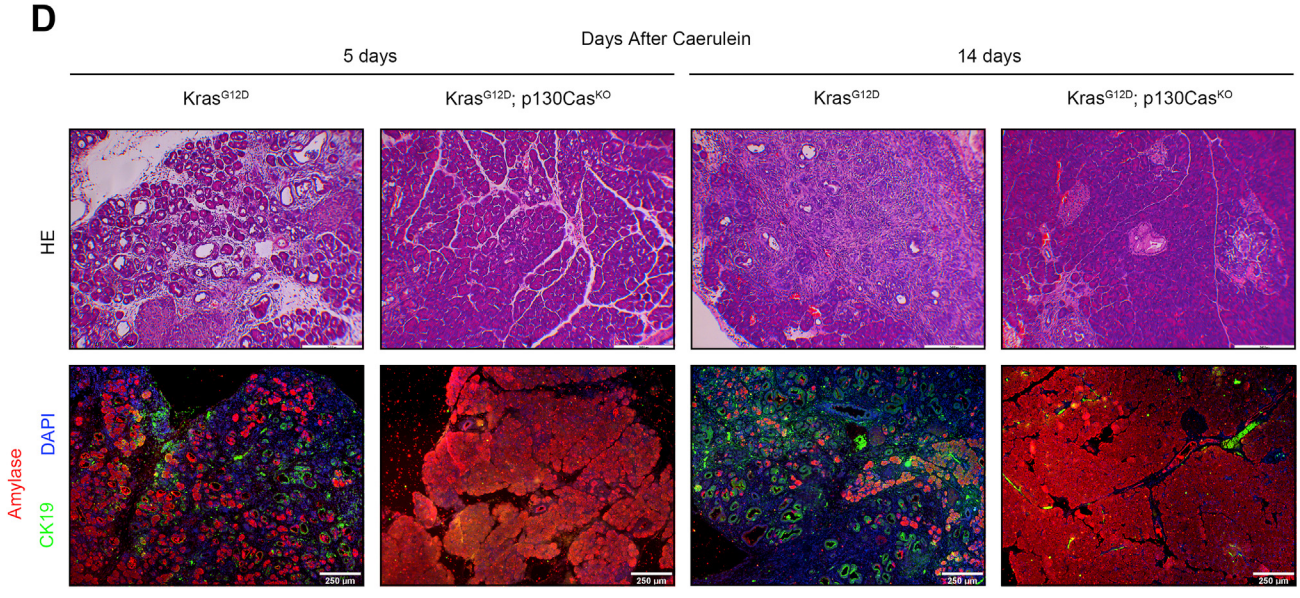
D
Days After Caerulein
5 days
14 days
KrasG12D
KrasG12D; p130CasKO
KrasG12D
KrasG12D; p130CasKO
HE
Amylase
CK19
DAPI
250 µm

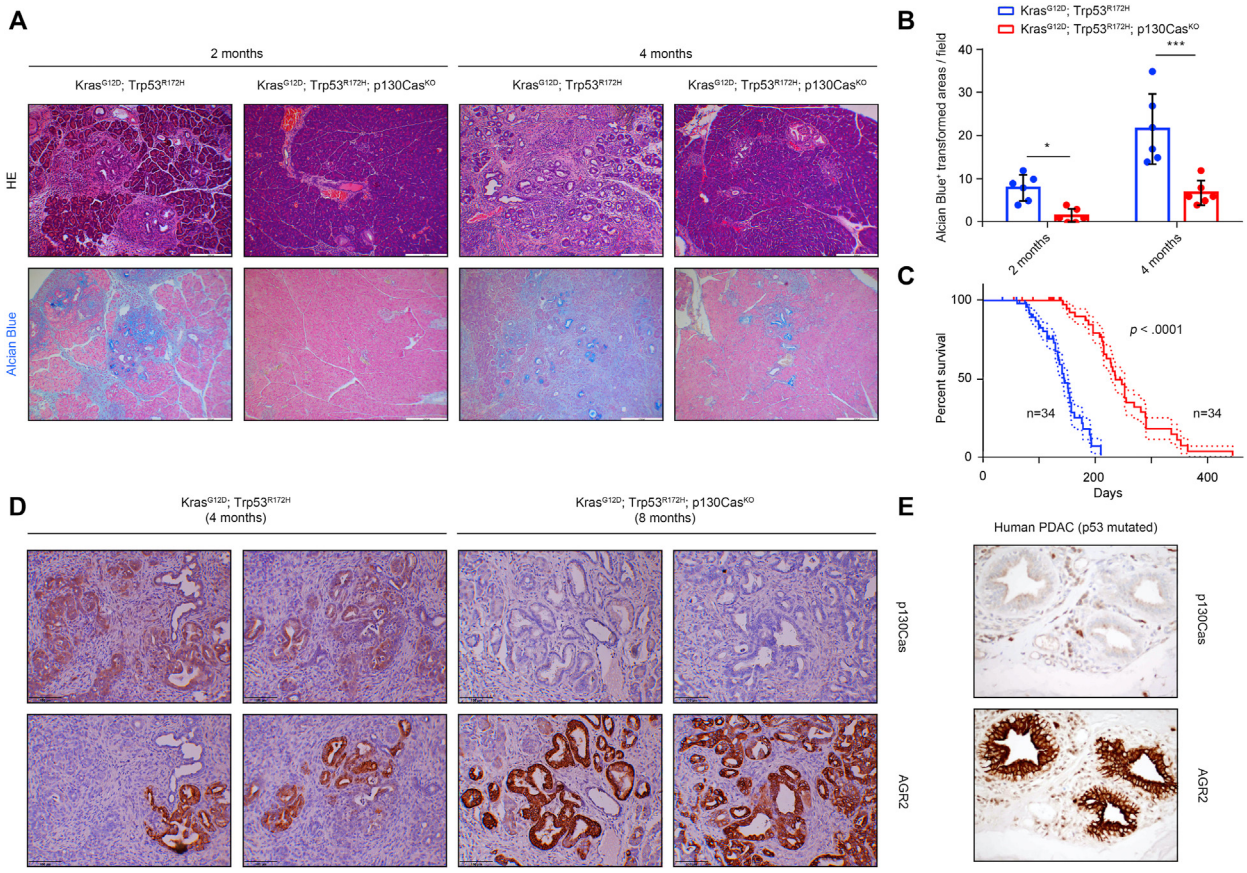

Figure 6. p130Cas expression is critical for acinar-derived PDAC. (*A*) Pancreatic tissue (normal acinar area and regions with ADM and PanINs) from $Kras^{G12D}$; $Trp53^{R172H}$ and $Kras^{G12D}$; $Trp53^{R172H}$; $p130Cas^{KO}$ mice was stained with H&E and Alcian Blue, as indicated. (*B*) Statistical analysis of Alcian Blue–positive lesions of pancreata from $Kras^{G12D}$; $Trp53^{R172H}$ (n = 6) and $Kras^{G12D}$; $Trp53^{R172H}$; $p130Cas^{KO}$ (n = 6) mice. Statistical analysis on Alcian Blue staining was performed with 2-way analysis of variance and presented as mean ± SD. $^{*}P < .05$; $^{***}P < .001$. (*C*) Kaplan–Meier survival curve between $Kras^{G12D}$; $Trp53^{R172H}$ (n = 34) and $Kras^{G12D}$; $Trp53^{R172H}$; $p130Cas^{KO}$ (n = 34) mice. Statistical analysis was performed with Mantel–Cox log-rank test. (*D*) Immunohistochemistry (IHC) for p130Cas and AGR2 in $Kras^{G12D}$; $Trp53^{R172H}$ and $Kras^{G12D}$; $Trp53^{R172H}$; $p130Cas^{KO}$ mice. (*E*) Representative results for IHC staining of p130Cas and AGR2 in a p130Cas-low human PDAC sample harboring p53 mutation.

in enzyme-linked immunosorbent assay (ELISA) measurements in tumor samples, patients with PDAC with low p130Cas expression also displayed reduced pAKT (Figure 4*E*) but not pERK1/2 (Supplementary Figure 3*G*). To further demonstrate that p130Cas mediated Kras-driven ADM through PI3K, we treated $Kras^{G12D}$ acini with the PI3K inhibitor LY294002. As reported in Figure 4*F* and *G*, LY294002 treatment (10 μM) completely suppressed Kras-dependent ADM and AKT phosphorylation (Supplementary Figure 3*H* and *I*) regardless of p130Cas expression levels.

This result showed that cell autonomous p130Cas expression supports PI3K–AKT signaling and permits Kras-induced ADM formation.

p130Cas Expression Is Necessary for $Kras^{G12D}$-Induced Acinar to Ductal Metaplasia and Acinar Tumorigenesis In Vivo

To test whether the role of p130Cas in ADM in vitro was also confirmed in vivo, we analyzed tumorigenesis in different models of PDAC with increasing aggressivity. First, $Kras^{G12D}$; $p130Cas^{KO}$ mice were allowed to age and examined for the presence of ADM and tumor lesions. In this context, p130Cas ablation prevented mouse lethality and the occurrence of Kras-induced lesions. As such, $p130Cas^{KO}$ animals retained a substantially normal pancreatic histology and function (Supplementary Figure 4*B*), as evaluated by mucin

Figure 5. p130Cas expression is necessary for $Kras^{G12D}$-induced ADM and acinar tumorigenesis. (*A*) Pancreatic tissue (normal acinar area and regions with ADM and PanINs) from $Kras^{G12D}$ and $Kras^{G12D}$; $p130Cas^{KO}$ mice was stained with H&E and Alcian Blue as indicated. (*B*) Statistical analysis of Alcian Blue–positive lesions from $Kras^{G12D}$ (n = 6) and $Kras^{G12D}$; $p130Cas^{KO}$ (n = 6) mice. (*C*) Kaplan–Meier survival curve between $Kras^{G12D}$ (n = 21) and $Kras^{G12D}$; $p130Cas^{KO}$ (n = 21) mice. Statistical analysis was performed with Mantel–Cox log-rank test. (*D*) Pancreatic tissue (normal acinar area and regions with ADM and PanINs) from $Kras^{G12D}$ and $Kras^{G12D}$; $p130Cas^{KO}$ mice after caerulein treatment was stained with H&E or analyzed by immunofluorescence for expression of amylase (*red*), CK19 (*green*), and 4′,6-diamidino-2-phenylindole (DAPI) (*blue*), as indicated. $^{***}P < .001$.

(Figure 5*A* and *B*), amylase/cytokeratin 19 (CK19) staining, and fibrotic collagen deposition (Supplementary Figure 4*A*, *C*, and *D*). The majority of $Kras^{G12D}$; $p130Cas^{KO}$ mice did not develop ADM or tumor lesions, even at 12 months of age, resulting in a significant improvement in survival (Figure 5*C*). Of note, only 5 $Kras^{G12D}$; $p130Cas^{KO}$ mice of 21 exhibited some rare ADM and occasional PanINs (Supplementary Figure 4*E* and *F*). These few PanINs were not due to incomplete loss of p130Cas, as lesions largely failed to express p130Cas when analyzed by immunohistochemistry.

These data demonstrate that p130Cas is an essential effector for Kras-driven ADM and subsequent tumorigenesis.

Pancreatic Epithelial p130Cas Deletion Inhibits Pancreatitis-Induced Acinar to Ductal Metaplasia

Pancreatitis synergizes with Kras-induced tumorigenesis by forcing acinar cells into ADM and exacerbating tumor initiation.[28] We thus explored the in vivo requirement of acinar p130Cas expression for ADM formation in pancreatic tissue injury alone or in the concomitant presence of $Kras^{G12D}$. In non-Kras–mutated pancreata, loss of p130Cas reduced ADM formation triggered by caerulein after 1 day of treatment, as evaluated by the reduced number of CK19-positive structures (Supplementary Figure 5*A*). To test whether p130Cas was also required for Kras-induced ADM formation in the setting of pancreatitis, we treated $Kras^{G12D}$ and $Kras^{G12D}$; $p130Cas^{KO}$ with caerulein. By 5 days after caerulein injection, the exocrine compartment of $Kras^{G12D}$ mice was almost completely replaced by fibrosis (Supplementary Figure 5*B* and *C*) and ductal structures, as evident by rare expression of the acinar marker amylase (Figure 5*D* and Supplementary Figure 5*C*). In stark contrast, pancreata of $Kras^{G12D}$; $p130Cas^{KO}$ mice did not display gross fibrosis and ADM after caerulein treatment and retained dramatically more amylase-positive parenchyma.

Our data demonstrate that p130Cas deletion was sufficient to prevent ADM on tissue injury alone or in combination with $Kras^{G12D}$ mutation.

p130Cas Expression Is Critical for Acinar-Derived Pancreatic Ductal Adenocarcinoma

Finally, we tested whether the loss of p130Cas affects tumor development in a model where cancer initiation is accelerated by concomitant inactivation of the p53 tumor suppressor.[27] In this aggressive tumor model, p130Cas ablation reduced the number of tumor lesions at 4 months of age, suggesting a delay in tumor onset (Figure 6*A* and *B*). To validate this hypothesis, a cohort of $Kras^{G12D}$; $Trp53^{R172H}$ and $Kras^{G12D}$; $Trp53^{R172H;}$ $p130Cas^{KO}$ animals were sacrificed at 2 months of age, when, in this tumor model, PanIN lesions start to develop. Counting of lesions confirmed a substantial delay in tumor onset for $Kras^{G12D}$; $Trp53^{R172H;}$ $p130Cas^{KO}$ mice (Figure 6*A* and *B*). Accordingly, survival of $Kras^{G12D}$; $Trp53^{R172H}$ mice was significantly extended by genetic ablation of p130Cas (Figure 6*C*).

Given that the $Kras^{G12D}$; $Trp53^{R172H}$ genotype can lead to ADM as well as direct transformation of ductal cells,[6,7,9,10] we next tested whether the loss of p130Cas modified ADM even in the presence of mutant p53. To this aim, we stained for the ductal cell marker AGR2 (anterior gradient protein 2), which can trace tumor origin and distinguish between lesions formed by either ADM or direct ductal cell transformation.[43] Tumors from $Kras^{G12D}$; $Trp53^{R172H}$; $p130Cas^{WT}$ mice exhibited the expected mixed positive and negative AGR2 staining (Figure 6*D*, *left panel* and Supplementary Figure 5*D*). On the contrary, $p130Cas^{KO}$ tumors appeared uniformly positive for AGR2 (Figure 6*D*, *right panel* and Supplementary Figure 5*D*), indicating that p130Cas deletion blocked ADM, but did not arrest direct transformation of ductal cells. Likewise, p53-mutated human PDAC tissue sections with low p130Cas staining showed strong AGR2 expression (Figure 6*E*), indicating that reduced expression of p130Cas impaired ADM in mice as well as in patients.

Discussion

PDAC is believed to develop in a gradual manner,[44] but early detection is challenging, and late diagnosis is one of the major reasons for the high mortality. A better understanding of the early events that lead to PDAC is crucial. ADM is now established as an important precursor to PanIN lesions and progression to pancreatic cancer, but our understanding of the mechanisms that drive this process remain incomplete.[5–7] In the present study, we demonstrated the pivotal role of p130Cas expression during acinar metaplasia through the regulation of PI3K–AKT pathway. We detected increased p130Cas expression in patients with early-stage PDAC, suggesting that p130Cas might be crucial to promote early PDAC development. Accordingly, patients with high p130Cas expression displayed poorer prognosis and lower survival, highlighting the impact that the initial phases have on the entire course of the disease. Future investigations might uncover the molecular mechanisms that drive p130Cas overexpression in these patients and how this affects tumor evolution.

Our data from $Kras^{G12D}$ mice demonstrated that the increase of p130Cas levels concurs with the metaplastic transition of acinar cells toward ductal intermediates. However, p130Cas up-regulation during ADM was not restricted to $Kras^{G12D}$ cells only because it also happened in normal acini after caerulein or EGF treatment. In this condition of pancreatic injury, ADM as well as p130Cas overexpression appears to be a temporary acinar response that physiologically resolves with pancreatic repair over time.[6,45] However, the metaplastic transition primes acinar cells to $Kras^{G12D}$ oncogenic transformation that promotes the formation of pre-invasive lesions.[46] Interestingly, we demonstrated that increasing p130Cas levels also increased $Kras^{G12D}$-induced ADM, providing a possible explanation for the poorer prognosis of patients with p130Cas overexpression.

The expression of mutant $Kras^{G12D}$ in the murine pancreas is sufficient to initiate ADM and lock metaplastic cells in a duct-like state.[26] However, this occurs with low penetrance and long latency, explaining why secondary events are required for

efficient ADM induction and transformation of pancreatic acinar cells, such as additional genetic lesions, chronic inflammation, or up-regulation of growth factor signaling.[6,7,28] Previous studies showed that both EGFR and Kras signaling converge to elevate PI3K activity and to induce acinar metaplasia.[47] Specifically, the signaling mediated by EGFR is still essential to promote the activation of PI3K–AKT pathway that is not fully activated by resident mutant Kras.[37,47,48]

Mechanistically, the activation of PI3K signaling by $Kras^{G12D}$ is mediated by its direct binding to p110 catalytic subunit.[49] Nevertheless, the interaction of p85α regulatory subunit with phosphotyrosines is still required to achieve full activation of the PI3K–AKT pathway.[50,51] Phosphorylated-p130Cas interacts with p85α in v-Crk (Avian Sarcoma Virus CT10 Oncogene Homolog)–transformed cells, where it promotes PI3K activity.[41,42] In line with this finding, we demonstrated that, in our cellular model, phosphorylated-p130Cas binds to p85α and allows full PI3K–AKT activation by oncogenic Kras. Accordingly, we found that loss of p130Cas decreased PI3K activity downstream of $Kras^{G12D}$ and EGFR. Inactivation of p110α is sufficient to block ADM induced by inflammation and oncogenic Kras, thereby suppressing pancreatic cancer initiation.[39] In agreement, the same phenotypes were recapitulated by p130Cas deletion in mouse models. Our data demonstrated that loss of p130Cas was sufficient to prevent ADM on caerulein-induced tissue injury alone or in combination with $Kras^{G12D}$ mutation, resulting in complete protection from single $Kras^{G12D}$ mutation.

Besides the PI3K–AKT axis, other pathways might be controlled by p130Cas during Kras-dependent tumorigenesis and progression, including, for example, the DOCK1–RAC1–β-catenin axis and Myc down-regulation[21] or the activation of FAK and integrin signaling.[17,52] In our study, we successfully confirmed that p130Cas deletion reduces Myc expression, but this down-regulation was mild and β-catenin activation was not affected. Although seemingly in contrast with previous reports,[21] different experimental conditions might explain the potential discrepancy; for example, our 3D cultured primary acini, isolated before Kras acinar metaplasia, did not proliferate at the rate detected in 2-dimensional–grown, fully transformed cancer cell lines. In addition, our 3D-grown p130Cas-deficient acinar cells showed that FAK activation was unexpectedly normal. Although p130Cas is an important component of the integrin signaling cascade and a sensitive mechanosensory,[53,54] it is possible that our cell culture conditions modified adhesion-mediated signaling. Although other adaptor proteins, for example, Paxillin,[52,55] might have replaced p130Cas in 3D cultures, further studies are needed to fully understand why the loss of p130Cas appears to mainly affect the PI3K pathway and no other signaling cascades.

In the $Kras^{G12D}$ mouse model, tumors arise predominantly from acinar cells through ADM and PanIN progression because ductal cells require additional Trp53 mutation to be transformed efficiently.[9] Remarkably, detection of the AGR2 protein could stratify double Kras-Trp53 mutant tumors according to the cell of origin, as this marker is expressed mainly in ductal-derived lesions and absent in acinar-derived lesions.[43] Our analysis of AGR2 expression indicated that deletion of p130Cas delayed tumor onset and forced tumors toward a ductal origin, as evident by the uniform AGR2 staining. These data indicate that acinar cell transformation depends on p130Cas expression, even in the absence of functional Trp53. Nevertheless, ductal cells bypass the requirement of p130Cas and form tumors at later time points, eventually reducing mouse survival. Notably, the effect of p130Cas deletion is reminiscent of the impact of EGFR ablation in a comparable tumor model without functional Trp53 ($Ptf1a^{Cre}$; $Kras^{G12D}$; $Trp53^{fl/fl}$).[47] Similarly to our triple-mutant mice, loss of EGFR in the Kras-Trp53 mutant background showed reduced PI3K–AKT signaling, blockage of Kras-dependent ADM, and incomplete protection from tumor development. Thus, $EGFR^{KO}$ PDAC might originate similarly to $p130Cas^{KO}$ tumors through direct ductal cell transformation. Furthermore, and in agreement with our results, genetic inactivation of the PI3K subunit p110α results in full suppression of tumor onset, demonstrating the central role of the PI3K pathway in PDAC development.[39] Thus, our findings concur with the notion that PI3K activity must be inactivated to prevent transformation of the ductal compartment.

Our work highlights the importance of identifying the pancreatic cell type originating PDAC to guide specific intervention in patients. Furthermore, the emerging efficacy of PI3K pathway inhibitors, as well as the identification of suitable biomarkers for patient stratification, like p130Cas, can move PDAC toward a precision medicine approach.

Supplementary Material

Note: To access the supplementary material accompanying this article, visit the online version of *Gastroenterology* at www.gastrojournal.org, and at http://doi.org/10.1053/j.gastro.2021.12.242.

References

1. Neoptolemos JP, Kleeff J, Michl P, et al. Therapeutic developments in pancreatic cancer: current and future perspectives. Nat Rev Gastroenterol Hepatol 2018; 15:333–348.
2. Siegel RL, Miller KD, Jemal A. Cancer statistics, 2020. CA Cancer J Clin 2020;70:7–30.
3. Buscail L, Bournet B, Cordelier P. Role of oncogenic KRAS in the diagnosis, prognosis and treatment of pancreatic cancer. Nat Rev Gastroenterol Hepatol 2020; 17:153–168.
4. Habbe N, Shi G, Meguid RA, et al. Spontaneous induction of murine pancreatic intraepithelial neoplasia (mPanIN) by acinar cell targeting of oncogenic Kras in adult mice. Proc Natl Acad Sci U S A 2008;105:18913–18918.
5. Bailey JM, DelGiorno KE, Crawford HC. The secret origins and surprising fates of pancreas tumors. Carcinogenesis 2014;35:1436–1440.
6. Storz P. Acinar cell plasticity and development of pancreatic ductal adenocarcinoma. Nat Rev Gastroenterol Hepatol 2017;14:296–304.

7. Storz P, Crawford HC. Carcinogenesis of pancreatic ductal adenocarcinoma. Gastroenterology 2020; 158:2072–2081.
8. Bailey P, Chang DK, Nones K, et al. Genomic analyses identify molecular subtypes of pancreatic cancer. Nature 2016;531:47–52.
9. Kopp JL, von Figura G, Mayes E, et al. Identification of Sox9-dependent acinar-to-ductal reprogramming as the principal mechanism for initiation of pancreatic ductal adenocarcinoma. Cancer Cell 2012;22:737–750.
10. Lee AYL, Dubois CL, Sarai K, et al. Cell of origin affects tumour development and phenotype in pancreatic ductal adenocarcinoma. Gut 2019;68:487–498.
11. Ray KC, Bell KM, Yan J, et al. Epithelial tissues have varying degrees of susceptibility to KrasG12D-initiated tumorigenesis in a mouse model. PLoS One 2011;6: e16786.
12. von Figura G, Morris JP, Wright CVE, et al. Nr5a2 maintains acinar cell differentiation and constrains oncogenic Kras-mediated pancreatic neoplastic initiation. Gut 2014;63:656–664.
13. Flandez M, Cendrowski J, Cañamero M, et al. Nr5a2 heterozygosity sensitises to, and cooperates with, inflammation in KRasG12V-driven pancreatic tumourigenesis. Gut 2014;63:647–655.
14. Childs EJ, Mocci E, Campa D, et al. Common variation at 2p13.3, 3q29, 7p13 and 17q25.1 associated with susceptibility to pancreatic cancer. Nat Genet 2015; 47:911–916.
15. Wolpin BM, Rizzato C, Kraft P, et al. Genome-wide association study identifies multiple susceptibility loci for pancreatic cancer. Nat Genet 2014;46:994–1000.
16. Zhong J, Jermusyk A, Wu L, et al. A transcriptome-wide association study (TWAS) identifies novel candidate susceptibility genes for pancreatic cancer. J Natl Cancer Inst 2018;7:5727–5732.
17. Cabodi S, del Pilar Camacho-Leal M, Di Stefano P, et al. Integrin signalling adaptors: not only figurants in the cancer story. Nat Rev Cancer 2010;10:858–870.
18. Defilippi P, Di Stefano P, Cabodi S. p130Cas: a versatile scaffold in signaling networks. Trends Cell Biol 2006; 16:257–263.
19. Tikhmyanova N, Little JL, Golemis EA. CAS proteins in normal and pathological cell growth control. Cell Mol Life Sci 2010;67:1025–1048.
20. Tornillo G, Defilippi P, Cabodi S. Cas proteins: dodgy scaffolding in breast cancer. Breast Cancer Res 2014; 16:443.
21. Waters AM, Khatib TO, Papke B, et al. Targeting p130Cas- and microtubule-dependent MYC regulation sensitizes pancreatic cancer to ERK MAPK inhibition. Cell Rep 2021;35(13):109291.
22. Pei H, Li L, Fridley BL, et al. FKBP51 affects cancer cell response to chemotherapy by negatively regulating Akt. Cancer Cell 2009;16:259–266.
23. Yang S, He P, Wang J, et al. A novel MIF signaling pathway drives the malignant character of pancreatic cancer by targeting NR3C2. Cancer Res 2016; 76:3838–3850.
24. Zhang G, He P, Tan H, et al. Integration of metabolomics and transcriptomics revealed a fatty acid network exerting growth inhibitory effects in human pancreatic cancer. Clin Cancer Res 2013;19:4983–4993.
25. Sciarrillo R, Wojtuszkiewicz A, El Hassouni B, et al. Splicing modulation as novel therapeutic strategy against diffuse malignant peritoneal mesothelioma. EBioMedicine 2019;39:215–225.
26. Hingorani SR, Petricoin EF, Maitra A, et al. Preinvasive and invasive ductal pancreatic cancer and its early detection in the mouse. Cancer Cell 2003;4:437–450.
27. Hingorani SR, Wang L, Multani AS, et al. Trp53R172H and KrasG12D cooperate to promote chromosomal instability and widely metastatic pancreatic ductal adenocarcinoma in mice. Cancer Cell 2005;7:469–483.
28. Guerra C, Schuhmacher AJ, Cañamero M, et al. Chronic pancreatitis is essential for induction of pancreatic ductal adenocarcinoma by K-Ras oncogenes in adult mice. Cancer Cell 2007;11:291–302.
29. Friedlander SYG, Chu GC, Snyder EL, et al. Context-dependent transformation of adult pancreatic cells by oncogenic K-Ras. Cancer Cell 2009;16:379–389.
30. Hong X, Zhang J, Wu Q, et al. Challenges in detecting pre-malignant pancreatic lesions during acute pancreatitis using a serum microRNA assay: a study based on KrasG12D transgenic mice. Oncotarget 2016; 7:22700–22710.
31. Norberg KJ, Nania S, Li X, et al. RCAN1 is a marker of oxidative stress, induced in acute pancreatitis. Pancreatology 2018;18:734–741.
32. Ulmasov B, Oshima K, Rodriguez MG, et al. Differences in the degree of cerulein-induced chronic pancreatitis in C57BL/6 mouse substrains lead to new insights in identification of potential risk factors in the development of chronic pancreatitis. Am J Pathol 2013; 183:692–708.
33. Means AL, Meszoely IM, Suzuki K, et al. Pancreatic epithelial plasticity mediated by acinar cell transdifferentiation and generation of nestin-positive intermediates. Development 2005;132:3767–3776.
34. Paoli C, Carrer A. Organotypic culture of acinar cells for the study of pancreatic cancer initiation. Cancers (Basel) 2020;12:1–22.
35. del Pilar Camacho Leal M, Costamagna A, Tassone B, et al. Conditional ablation of p130Cas/BCAR1 adaptor protein impairs epidermal homeostasis by altering cell adhesion and differentiation. Cell Commun Signal 2018;16:73.
36. Honda H, Oda H, Nakamoto T, et al. Cardiovascular anomaly, impaired actin bundling and resistance to Src-induced transformation in mice lacking p130(Cas). Nat Genet 1998;19:361–365.
37. Navas C, Hernández-Porras I, Schuhmacher AJ, et al. EGF receptor signaling Is essential for K-Ras oncogene-driven pancreatic ductal adenocarcinoma. Cancer Cell 2012;22:318–330.
38. Eser S, Reiff N, Messer M, et al. Selective requirement of PI3K/PDK1 signaling for kras oncogene-driven pancreatic cell plasticity and cancer. Cancer Cell 2013; 23:406–420.

39. Baer R, Cintas C, Dufresne M, et al. Pancreatic cell plasticity and cancer initiation induced by oncogenic Kras is completely dependent on wild-type PI 3-kinase p110α. Genes Dev 2014;28:2621–2635.
40. Carrer A, Trefely S, Zhao S, et al. Acetyl-CoA metabolism supports multistep pancreatic tumorigenesis. Cancer Discov 2019;9:416–435.
41. Li E, Stupack DG, Brown SL, et al. Association of p130CAS with phosphatidylinositol-3-OH kinase mediates adenovirus cell entry. J Biol Chem 2000; 275:14729–14735.
42. Riggins RB, DeBerry RM, Toosarvandani MD, et al. Src-dependent association of Cas and p85 phosphatidylinositol 3'-kinase in v-crk-transformed cells. Mol Cancer Res 2003;1:428–437.
43. Ferreira RMM, Sancho R, Messal HA, et al. Duct- and acinar-derived pancreatic ductal adenocarcinomas show distinct tumor progression and marker expression. Cell Rep 2017;21:966–978.
44. Yachida S, Jones S, Bozic I, et al. Distant metastasis occurs late during the genetic evolution of pancreatic cancer. Nature 2010;467:1114–1117.
45. Giroux V, Rustgi AK. Metaplasia: tissue injury adaptation and a precursor to the dysplasia-cancer sequence. Nat Rev Cancer 2017;17:594–604.
46. Li Y, He Y, Peng J, et al. Mutant Kras co-opts a proto-oncogenic enhancer network in inflammation-induced metaplastic progenitor cells to initiate pancreatic cancer. Nat Cancer 2021;2:49–65.
47. Ardito CM, Grüner BM, Takeuchi KK, et al. EGF receptor is required for KRAS-induced pancreatic tumorigenesis. Cancer Cell 2012;22:304–317.
48. Blasco MT, Navas C, Martín-Serrano G, et al. Complete regression of advanced pancreatic ductal adenocarcinomas upon combined inhibition of EGFR and C-RAF. Cancer Cell 2019;35:573–587.e6.
49. Castellano E, Downward J. RAS interaction with PI3K: more than just another effector pathway. Genes Cancer 2011;2:261–274.
50. Jiménez C, Hernández C, Pimentel B, et al. The p85 regulatory subunit controls sequential activation of phosphoinositide 3-kinase by Tyr kinases and Ras. J Biol Chem 2002;277:41556–41562.
51. Fruman DA, Chiu H, Hopkins BD, et al. The PI3K pathway in human disease. Cell 2017;170:605–635.
52. Katoh K. FAK-dependent cell motility and cell elongation. Cells 2020;9:192.
53. Janoštiak R, Pataki AC, Brábek J, et al. Mechanosensors in integrin signaling: the emerging role of p130Cas. Eur J Cell Biol 2014;93:445–454.
54. Sawada Y, Tamada M, Dubin-Thaler BJ, et al. Force sensing by mechanical extension of the Src family kinase substrate p130Cas. Cell 2006;127:1015–1026.
55. Nakamura K, Yano H, Uchida H, et al. Tyrosine phosphorylation of paxillin α is involved in temporospatial regulation of paxillin-containing focal adhesion formation and F-actin organization in motile cells. J Biol Chem 2000;275:27155–27164.

Received June 29, 2021. Accepted December 12, 2021.

Correspondence
Address correspondence to: Andrea Costamagna, PhD, Molecular Biotechnology Center, Department of Molecular Biotechnology and Health Sciences, University of Torino, Via Nizza 52, 10126, Torino, Italy. e-mail: a.costamagna@unito.it; or Paola Defilippi, PhD, Molecular Biotechnology Center, Department of Molecular Biotechnology and Health Sciences, University of Torino, Via Nizza 52, 10126, Torino, Italy. e-mail: paola.defilippi@unito.it; or Emilio Hirsch, PhD, Molecular Biotechnology Center, Department of Molecular Biotechnology and Health Sciences, University of Torino, Via Nizza 52, 10126, Torino, Italy. e-mail: emilio.hirsch@unito.it; or Sara Cabodi, PhD, Molecular Biotechnology Center, Department of Molecular Biotechnology and Health Sciences, University of Torino, Via Nizza 52, 10126, Torino, Italy. e-mail: sara.cabodi@unito.it; or Miriam Martini, PhD, Molecular Biotechnology Center, Department of Molecular Biotechnology and Health Sciences, University of Torino, Via Nizza 52, 10126, Torino, Italy. e-mail: miriam.martini@unito.it.

Acknowledgments
The authors would like to thank Dr Paolo Ettore Porporato and Dr Alessandro Carrer for critically reading the manuscript and useful discussion.

CRediT Authorship Contributions
Andrea Costamagna, PhD (Conceptualization: Equal; Data curation: Lead; Formal analysis: Lead; Investigation: Lead; Writing – original draft: Lead).
Dora Natalini, MS (Data curation: Equal; Investigation: Equal; Writing – review & editing: Equal).
Maria del Pilar Camacho Leal, PhD (Conceptualization: Equal; Investigation: Equal).
Matilde Simoni, MS (Investigation: Equal).
Luca Gozzelino, MS (Investigation: Equal).
Paola Cappello, PhD (Data curation: Equal; Methodology: Equal).
Francesco Novelli, PhD (Data curation: Equal; Methodology: Equal).
Chiara Ambrogio, PhD (Methodology: Equal; Resources: Equal; Visualization: Equal).
Paola Defilippi, PhD (Formal analysis: Equal; Visualization: Equal).
Emilia Turco, MS (Methodology: Equal; Resources: Equal).
Elisa Giovannetti, MD, PhD (Conceptualization: Equal; Investigation: Equal; Methodology: Equal; Resources: Equal; Validation: Equal; Writing – original draft: Equal).
Emilio Hirsch, PhD (Funding acquisition: Equal; Visualization: Equal; Writing – review & editing: Equal).
Sara Cabodi, PhD (Conceptualization: Equal; Funding acquisition: Lead; Supervision: Equal).
Miriam Martini, PhD (Conceptualization: Equal; Funding acquisition: Lead; Supervision: Equal).

Conflicts of interest
This author discloses the following: Emilio Hirsch is a founder of Kither Biotech, a company involved in the development of PI3K inhibitors. The remaining authors disclose no conflicts.

Funding
Sara Cabodi's laboratory is supported by Associazione Italiana per la Ricerca sul Cancro AIRC (IG11346). Miriam Martini is supported by a Worldwide Cancer Research grant (WWCR 20-0033). Emilio Hirsch is supported by AIRC (IG21875), Ministero Università Ricerca (PRIN 2017), and Leducq Transatlantic Network of Excellence (19CVD02). Elisa Giovannetti is supported by AIRC (IG24444) and Dutch Cancer Society (KWF-11957). Chiara Ambrogio's laboratory is supported by the Giovanni Armenise–Harvard Foundation and the Lung Cancer Research Foundation. Paola Defilippi is supported by AIRC (IG-20107), Compagnia San Paolo Torino (Progetto DEFLECT), Fondazione CRT (2020.1798).

Supplementary Materials and Methods

Mice

The LSL-Kras^{G12D} and LSL-p53^{R172H} knock-in (from D. Tuveson, Mouse Models of Human Cancers Consortium repository, National Cancer Institute-Frederick), Pdx1^{Cre} (from D.A. Melton, Harvard University, Cambridge, MA) and p130Cas$^{fl/fl}$ (from S. Cabodi, University of Torino) strains were interbred on a mixed background (SV129/C57Bl6) to obtain compound mutant Pdx^{Cre}; Kras^{G12D} (named Kras^{G12D}), Pdx^{Cre}; Kras^{G12D}; Trp53^{R172H} (named Kras^{G12D}; p53^{R172H}), Pdx^{Cre}; Kras^{G12D}; p130Cas^{KO} (named Kras^{G12D}; p130Cas^{KO}), Pdx^{Cre} Kras^{G12D}; p53$^{R172H;}$ p130Cas^{KO} (Kras^{G12D}; p53^{R172H}; p130Cas^{KO}). Pdx1^{Cre} mice of the same age were used as controls. All procedures and animal housing conformed to the regulatory standards and were approved by the ethical committee according to the Guide for the Care and Use of Laboratory Animals published by the U.S. National Institutes of Health and approved by the Italian Health Minister (authorization no. 64-2016PR). Pancreatic injury was induced in young mice (8–12 weeks) by a series of six hourly intraperitoneal injections of cerulein (75 mg per kilogram of body weight) that was repeated after 48 hours. Animals were euthanized 1, 5, or 14 days later.

Preparation of Pancreatic Epithelial Explants Culture

The procedure to isolate primary pancreatic acinar cells was described in detail previously.[33,34] In brief, the pancreas was removed, washed twice with ice-cold Hank's balanced salt solution (HBSS) media, minced into 1–5 mm pieces and digested with collagenase I (37 °C, shaker). Collagen digestion was stopped by adding an equal volume of ice-cold HBSS media containing 5% fetal bovine serum (FBS). The digested pancreatic pieces were washed twice with HBSS media containing 5% FBS and then pipetted through 500 mm and then 105 mm meshes. The supernatant of the cell suspension containing acinar cells was added dropwise to 20 ml HBSS containing 30% FBS. Acinar cells were then pelleted (1,000 rpm, 2 min at 4°C), re-suspended in 10 ml RPMI complete media (1% FBS, 0.1 mg/ml trypsin inhibitor, 1 mg/ml dexamethasone) and plated into low-adhesion dishes for standard culture. For the 3D explant culture, cell culture plates were coated with collagen I. Isolated primary pancreatic acinar cells were added as a mixture with collagen I/medium media on the top of this layer. Further, complete media was added on top of the cell/gel mixture, replaced the following day and then every other day.

PI(3,4,5)P3 Quantification

Levels of PI(3,4,5)P3 were measured by ELISA kit (Echelon Bioscience, K2500) following manufacturer protocol.

Protein Analysis

Cells were homogenized in lysis buffer (120 mM NaCl, 50 mM Tris-HCl pH = 8, 1% Triton X-100) supplemented with 25x protease inhibitor cocktail (Roche), 50 mM sodium fluoride and 1 mM sodium orthovanadate. Lysates were cleared by centrifugation at 13,000 rpm for 15 min at 4°C. Protein concentration was determined by Bradford method and supernatants were analyzed for immunoblotting or for immunoprecipitation (IP) with the indicated antibodies. Membranes probed with the indicated antibodies were then incubated with HRP conjugated secondary antibodies (anti-mouse used 1:10000, anti-rabbit 1:5000, Sigma) and developed with enhanced chemiluminescence (ECL, Biorad). For IP assays, cells were lysed in IP lysis buffer (150 mM NaCl, 50 mM Tris [pH 7.5], 1% Igepal CA-630, 0.5% deoxycholate) and 1 mg of pre-cleared extracts were incubated with 1 μg of the indicated antibody at 4°C on a rotating rack overnight. Then 15 μl of protein G-Dynabeads (ThermoFisher) were added for 2 hours. Samples were collected by centrifugation (13,000 rpm 1 min) and washed six-times with IP lysis buffer. Bound protein complexes were then eluted by adding 30 μl Laemmli sample buffer.

Antibodies and Reagents

Cell treatments: recombinant murine EGF (PeproTech; #215-09; working concentration: 50 ng/ml unless otherwise specified), recombinant human TGFα (PeproTech; #100-16A; 50 ng/ml); LY294002 (Sigma Aldrich; #440202; 10 μM).

Mouse monoclonal antibodies to human/murine p130Cas were produced in our department. Additional p130Cas antibodies were purchased from BD Transduction Laboratory (Material number 610272) and Cell Signaling Technology (clone E1L9H, #13846). Antibodies against ERK1/2 (4696), P-ERK1/2 (4370), AKT (2920), P-AKT (9271 and 9277), pMEK1/2 (9121), MEK1/2 (4694), Myc (5605), Active β-Catenin (8814), Vinculin (4650), Tubulin (), GAPDH (2118), were from Cell Signaling Technology. Antibodies against Amylase (A8273), AGR2 (HPA007912), CK19 (MABT913) were from Sigma Aldrich.

Tissue Microarrays (TMAs), Immunohistochemistry (IHC) and Correlation With Clinical Outcome

To evaluate p130Cas as potential prognostic biomarker we selected a cohort of early stage patients (stage I–IIb, n = 95) treated with gemcitabine in the adjuvant setting. Representative cores of individual primary PDAC FFPE tissues prior to treatment were selected and combined in TMAs, as described previously.[e1] IHC staining of p130Cas was performed according to manufacturer's protocol. As negative control, slides stained with no primary antibody were used. Visualization was obtained with BenchMark Special Stain Automation system (Ventana Medical Systems, Export, USA). Staining was evaluated by a molecular pathologist, assessing the amount of tumor and tissue loss, background, and overall interpretability. Immunostaining intensity was classified into two grades: low and high p130Cas expression using a scoring system based on staining intensity and on the number of stained cells, as follows: immunostaining intensity was classified into four

grades: 0 (absent), 1 (weak), 2 (moderate), 3 (strong). We attributed one, two, or three additional points if the percentage of positive cells was less than 25%, 25% to 50%, or greater than 50%, respectively. Neoplastic cells were always uniformly stained and positivity assessment was made by counting all the tumor cells present in three tumor cores. All patients provided written informed consent for the storage, analysis of their tumor material and survival data. This study was approved by the Local Ethics Committee of the University of Pisa (Ethics approval #3909, 3 July 2013). Correlation with clinicopathological characteristics, including progression-free survival (PFS) and overall survival (OS), was tested with Kaplan–Meier curves and the log-rank test. Univariate analysis was performed and factors with a *P* value below 0.1 were evaluated in the multivariate analysis according to the Wald model, using SPSS software version 26 (IBM Corp, Armonk, NY). Statistical significance was set at *P* values below 0.05.

Histology and Immunohistochemistry

Normal tissues, pancreata, and cancer tissues of mice at specific age timepoints were fixed with 10% buffered formalin solution overnight and embedded into paraffin by the institutional pathology core laboratory.

Sections cut from paraffin block were stained with hematoxylin/eosin, Alcian Blue and PicroSirius Red following standard protocols. For immunolabeling, unstained 5-mm sections were cut from paraffin blocks and the slides deparaffinized by routine techniques followed by incubation in 1X sodium citrate antigen retrieval buffer (ThermoFisher) before steaming for 20 minutes in pressure cooker. Slides were cooled 2 hours, blocked, and incubated overnight with primary antibodies. Immunolabeling was detected using Novolink Polymer Detection System (Leica Biosystems), and sections were counterstained with hematoxylin. For immunolabeling, the staining intensity was scored and assigned based on this scale: 0 (absent), 1 (low positive signal), 2 (moderately strong positive signal), 3 (strong positive signal).

Tissue Extracts and Phospho-AKT and Phospho-ERK Enzyme-linked Immunosorbent Assays (ELISA)

Pancreatic levels of phospho-AKT and phospho-ERK were determined in stored supernatants from homogenized pancreatic cancer tissues by use of ELISA kits. In particular, the dual phosphorylation of ERK2 at threonine-185 and tyrosine-187 (ERK2 [pTpY185/187]) and ERK1 at threonine-202 and tyrosine-204 (ERK1 [pTpY202/204]) and the AKT phosphorylation at serine-473 (AKT [pS473]) were evaluated with specific ELISA assays (Invitrogen), as described previously.[e2] Selected frozen tissues from 8 PDAC patients with high and 8 PDAC patients with low p130Cas expression were collected and weighed in the same manner during preparation. Extract preparation was performed as recommended by the manufacturer. Briefly, each tissue sample was prepared with PBS and homogenized in cell lysis buffer (Cell Signaling Technology) containing Protease Inhibitor Cocktail. After incubation on ice for 30 minutes, the homogenate was centrifuged at 14,000 x g for 10 min at 4°C, and the supernatant was transferred to microtiter plates coated with monoclonal antibodies specific for phospho-AKT and phospho-ERK. Standard curves were run with each assay using 100, 50, 25, 12.5, 6.25, 3.12, and 1.6 U/ml phosphorylated full-length human recombinant phospho-AKT and phospho-ERK. After overnight incubation at 4°C, the solution was aspirated from wells, and 100 ml of rabbit anti-phospho-AKT or anti-phospho-ERK was added into each well. Plates were incubated at room temperature for 1 hour, washed four times, and 100 μl of a working solution of horseradish peroxidase-labeled anti-rabbit IgG was added into each well. After 30 minutes, a chromogen solution was added; 20 minutes later, the reactions were stopped with 100 μl of a stop solution, and the absorbance was read at 450 nm at 20 minutes intervals for 120 minutes to construct a plot of absorbance increase as a function of time. To calculate phospho-AKT and phospho-ERK concentrations, a standard curve method was used.

Patient-derived Expression Datasets

The following datasets were downloaded from the indicated source and used in the analyses: GSE16515, GSE62452, GSE28735, GSE41418, GSE109227, GSE77983.

Statistical Analysis

Prism software (GraphPad) was used for statistical analysis. Significance was calculated with Student *t* test and one- or two-way analysis of variance tests (ANOVA) followed by Bonferroni's post hoc analysis, or Mantel Cox log-rank test where appropriate. Values are reported as mean ± SD.

Supplementary References

e1. Giovannetti E, Wang Q, Avan A, et al. Role of CYB5A in pancreatic cancer prognosis and autophagy modulation. J Natl Cancer Inst 2014;106(1):djt346.

e2. Giovannetti E, Zucali PA, Assaraf YG, et al. Preclinical emergence of vandetanib as a potent antitumour agent in mesothelioma: molecular mechanisms underlying its synergistic interaction with pemetrexed and carboplatin. Br J Cancer 2011;105:1542–1553.

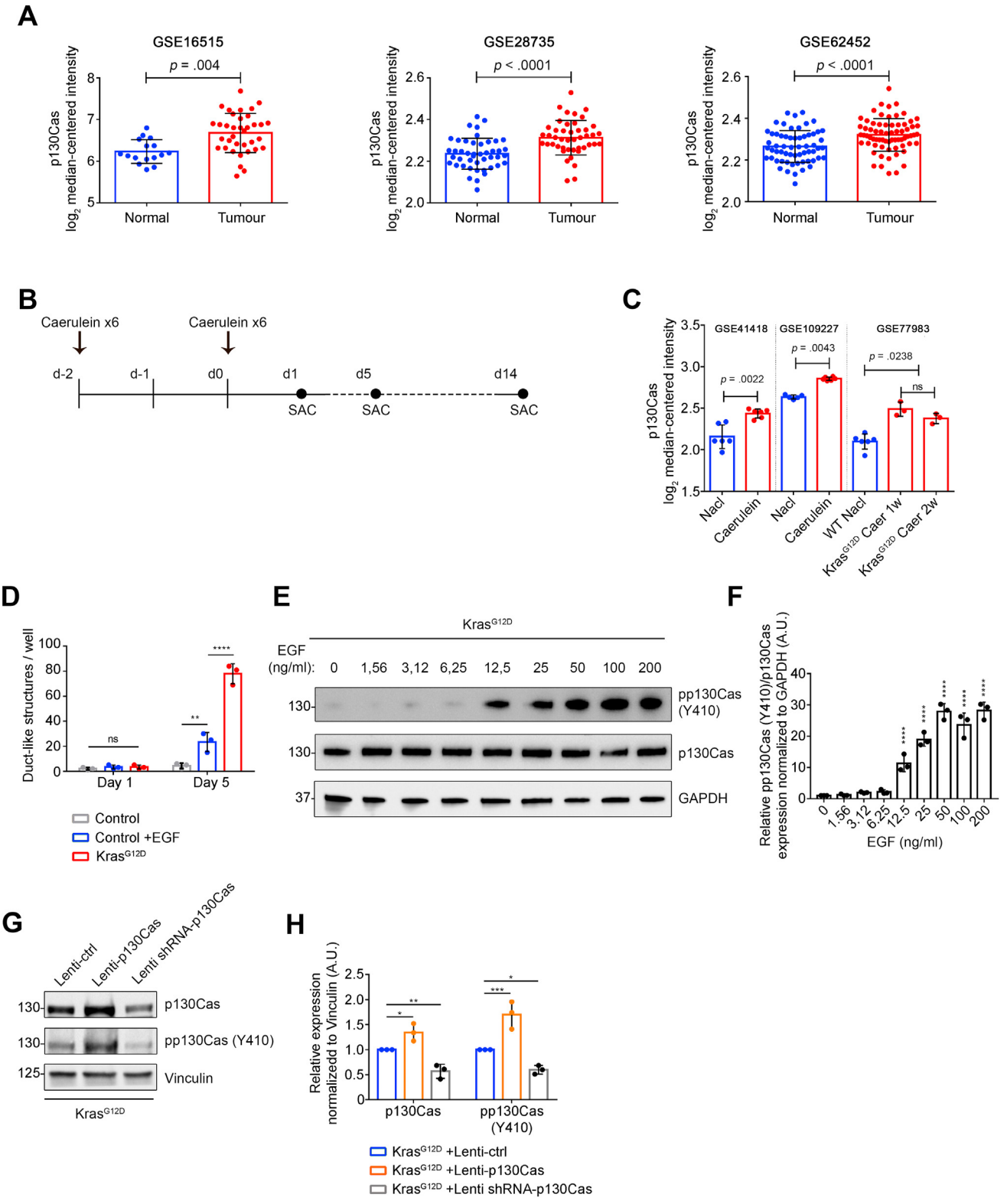
A
GSE16515
p = .004
p130Cas log2 median-centered intensity
Normal
Tumour
GSE28735
p < .0001
GSE62452
p < .0001
B
Caerulein x6
Caerulein x6
d-2
d-1
d0
d1
d5
d14
SAC
SAC
SAC
C
GSE41418
GSE109227
GSE77983
p = .0022
p = .0043
p = .0238
ns
Nacl
Caerulein
WT Nacl
KrasG12D Caer 1w
KrasG12D Caer 2w
D
Duct-like structures / well
Day 1
Day 5
Control
Control +EGF
KrasG12D
E
KrasG12D
EGF (ng/ml): 0 1,56 3,12 6,25 12,5 25 50 100 200
pp130Cas (Y410)
p130Cas
GAPDH
F
Relative pp130Cas (Y410)/p130Cas expression normalized to GAPDH (A.U.)
EGF (ng/ml)
G
Lenti-ctrl
Lenti-p130Cas
Lenti shRNA-p130Cas
p130Cas
pp130Cas (Y410)
Vinculin
KrasG12D
H
Relative expression normalizedd to Vinculin (A.U.)
p130Cas
pp130Cas (Y410)
KrasG12D +Lenti-ctrl
KrasG12D +Lenti-p130Cas
KrasG12D +Lenti shRNA-p130Cas

Supplementary Figure 1. (*A*) Log_2 median-centered p130Cas RNA expression in normal vs PDAC samples from indicated studies. Exact *P* values determined by Mann–Whitney test. (*B*) Scheme showing caerulein treatment and time points of mouse sacrifice. (*C*) Log_2 median-centered p130Cas RNA expression in saline-treated (n = 6) vs caerulein-treated mice (n = 6) (GSE41418), saline-treated (n = 5) vs caerulein-treated mice (n = 6) (GSE109227), or saline-treated (n = 6) vs caerulein-treated KrasG12D mice after 1 week (n = 3) or 2 weeks (n = 3) (GSE77983) samples from indicated studies. Exact *P* values determined by Mann–Whitney test or 1-way analysis of variance (ANOVA). (*D*) Quantification of the number of duct-like structures formed by murine pancreatic acini seeded in 3D collagen. (*E, F*) Primary acinar cultures were subjected to Western blot to evaluate p130Cas phosphorylation (pp130Cas Y410) in response to increasing EGF concentration, as indicated. (*G, H*) Western blot analysis of $Kras^{G12D}$ primary acinar cells transduced with lentiviral particles harboring ctrl, p130Cas or short hairpin RNA against p130Cas. Statistical analyses were performed with 2-way ANOVA and presented as mean ± SD. $^{*}P < .05$; $^{**}P < .01$; $^{***}P < .001$; $^{****}P < .0001$.

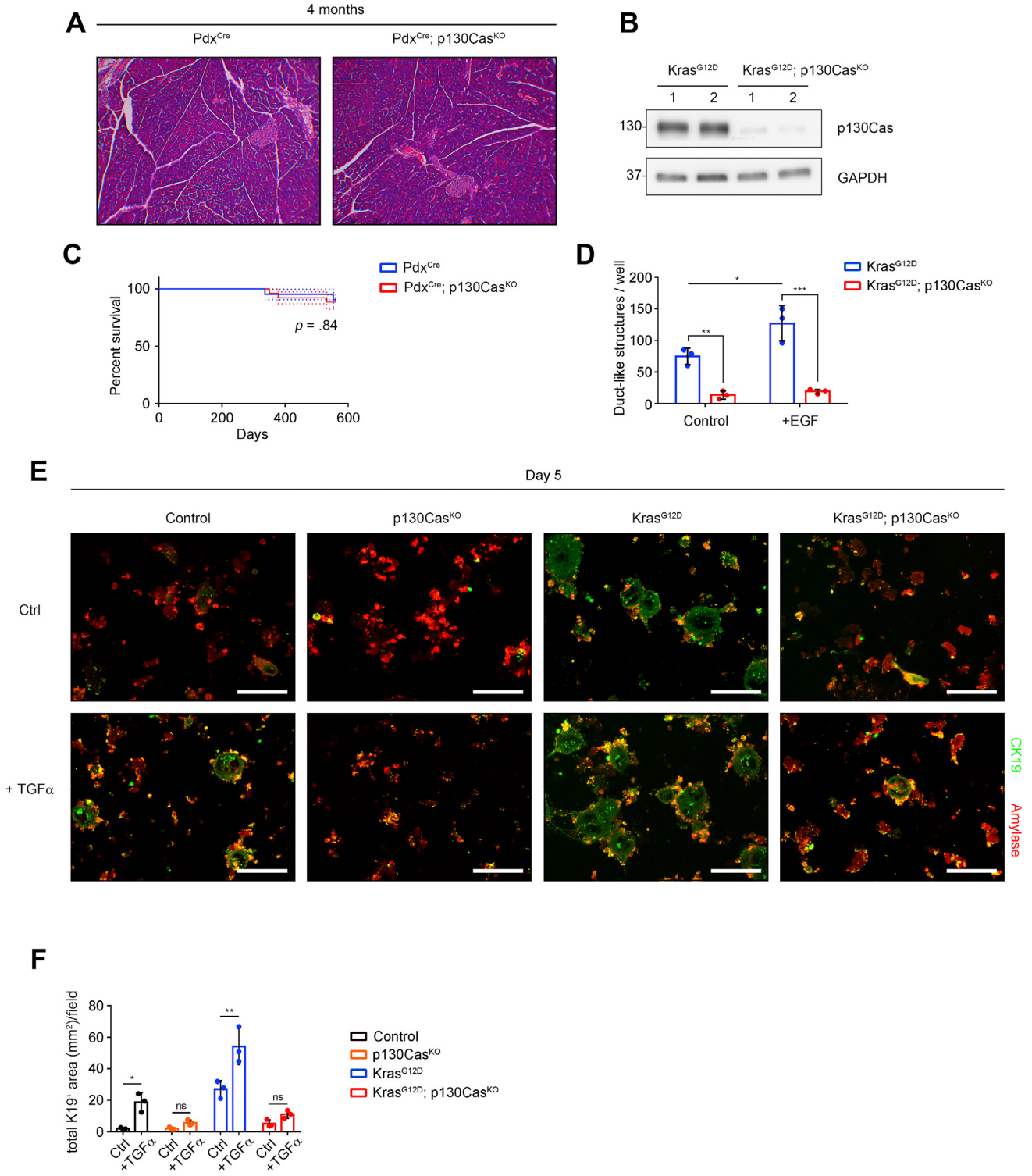

Supplementary Figure 2. (*A*) Pancreatic tissue from Pdx^{Cre} and Pdx^{Cre}; $p130Cas^{KO}$ mice was stained with H&E. (*B*) Western blot analysis of pancreatic lysates from Pdx^{Cre} and Pdx^{Cre}; $p130Cas^{KO}$ mice. (*C*) Kaplan–Meier survival curve between Pdx^{Cre} (n = 21) and Pdx^{Cre}; $p130Cas^{KO}$ (n = 24) mice. Statistical analysis was performed with Mantel–Cox log-rank test. (*D*) Quantification of the number of duct-like structures formed by murine pancreatic acini seeded in 3D collagen. (*E, F*) Primary acinar cells were isolated from murine pancreata of the indicated genotype, seeded in 3D culture in collagen and followed for transforming growth factor-α (TGFα)–induced transdifferentiation. Immunofluorescent staining revealed amylase-positive acinar cells (*red*) or CK19-positive ductal structures (ADM) (*green*). The area stained by CK19 was quantified to score ADM formation. Statistical analyses were performed with 2-way analysis of variance and presented as mean ± SD. $^{*}P < .05$; $^{**}P < .01$; $^{***}P < .001$.

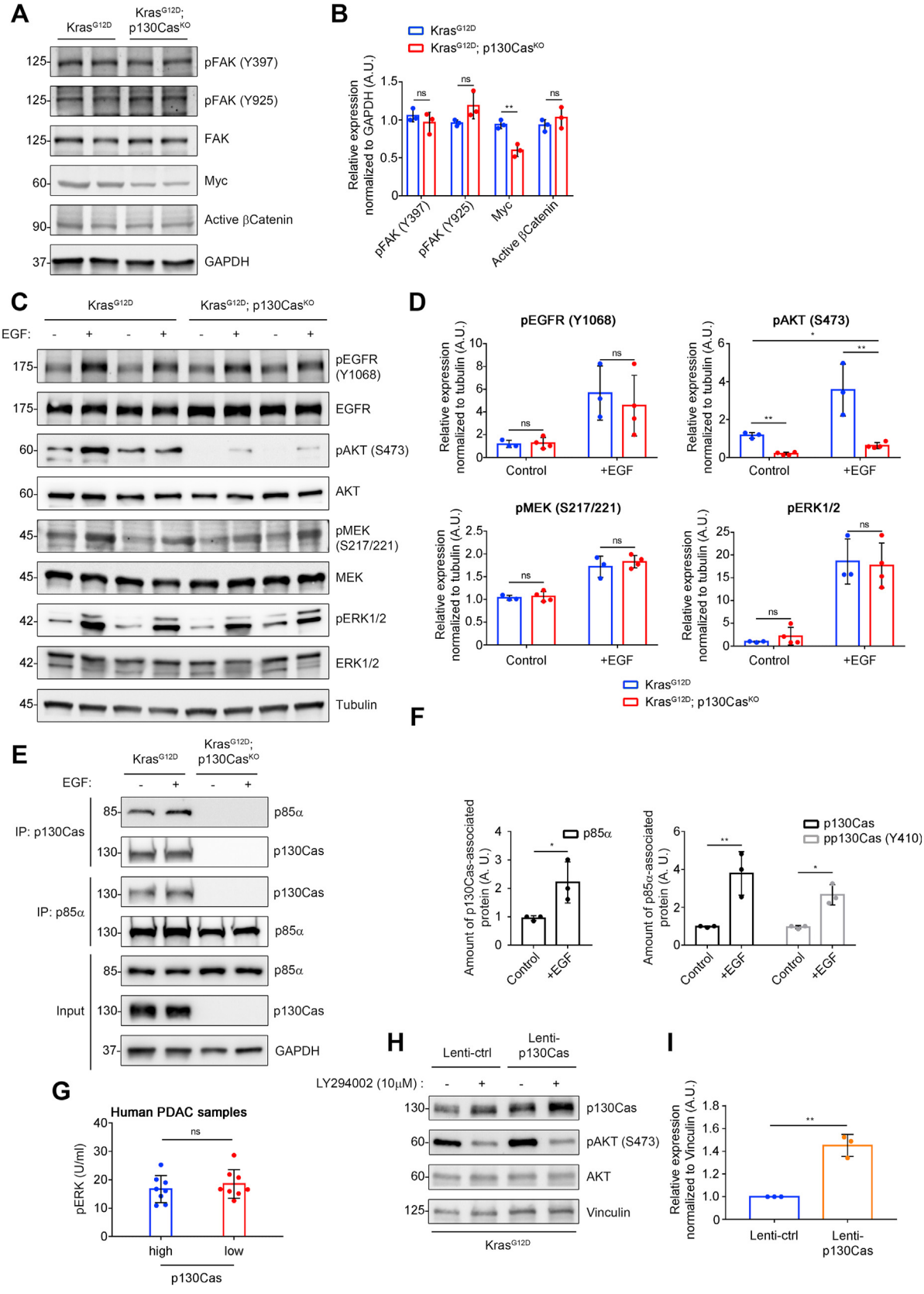
A
KrasG12D
KrasG12D; p130CasKO
125
pFAK (Y397)
125
pFAK (Y925)
125
FAK
60
Myc
90
Active βCatenin
37
GAPDH
B
KrasG12D
KrasG12D; p130CasKO
Relative expression normalized to GAPDH (A.U.)
ns
ns
**
ns
pFAK (Y397)
pFAK (Y925)
Myc
Active βCatenin
C
KrasG12D
KrasG12D; p130CasKO
EGF:
175
pEGFR (Y1068)
175
EGFR
60
pAKT (S473)
60
AKT
45
pMEK (S217/221)
45
MEK
42
pERK1/2
42
ERK1/2
45
Tubulin
D
pEGFR (Y1068)
pAKT (S473)
pMEK (S217/221)
pERK1/2
Relative expression normalized to tubulin (A.U.)
Control
+EGF
KrasG12D
KrasG12D; p130CasKO
E
KrasG12D
KrasG12D; p130CasKO
EGF:
IP: p130Cas
85
p85α
130
p130Cas
IP: p85α
130
p130Cas
130
p85α
Input
85
p85α
130
p130Cas
37
GAPDH
F
Amount of p130Cas-associated protein (A. U.)
p85α
Amount of p85α-associated protein (A. U.)
p130Cas
pp130Cas (Y410)
Control
+EGF
G
Human PDAC samples
pERK (U/ml)
ns
high
low
p130Cas
H
Lenti-ctrl
Lenti-p130Cas
LY294002 (10μM) :
130
p130Cas
60
pAKT (S473)
60
AKT
125
Vinculin
KrasG12D
I
Relative expression normalized to Vinculin (A.U.)
**
Lenti-ctrl
Lenti-p130Cas

Supplementary Figure 3. (*A, B*) Western blot analysis of primary acinar cells isolated from $Kras^{G12D}$ and $Kras^{G12D}$; $p130Cas^{KO}$ murine pancreata. Data reported are representative of at least 3 independent experiments. (*C, D*) Western blot analysis of primary acinar cells isolated from $Kras^{G12D}$ and $Kras^{G12D}$; $p130Cas^{KO}$ murine pancreata and treated with EGF, as indicated. Data reported are representative of at least 3 independent experiments. (*E*) Primary acinar cells isolated from mouse pancreas were treated with phosphate-buffered saline or EGF for 10 minutes and subjected to immunoprecipitation with anti-p130Cas and anti-p85α antibodies. p130Cas–p85α interaction was revealed by Western blot. (*F*) Quantification of p130Cas–p85α interaction from at least 3 independent immunoprecipitation experiments. (*G*) Quantification of pERK1/2 enzyme-linked immunosorbent assay (ELISA) from high p130cas ($n = 8$) and low p130Cas ($n = 8$) human PDAC samples. (*H, I*) Western blot analysis and quantification of primary acinar cells isolated from mouse pancreas, infected with lentiviral particles harboring ctrl or p130Cas and treated with LY294002 (10 μM) for 2 hours, as indicated. Statistical analyses were performed with 2-way analysis of variance and presented as mean $\pm$ SD. $^{*}P < .05$; $^{**}P < .01$; $^{***}P < .001$.

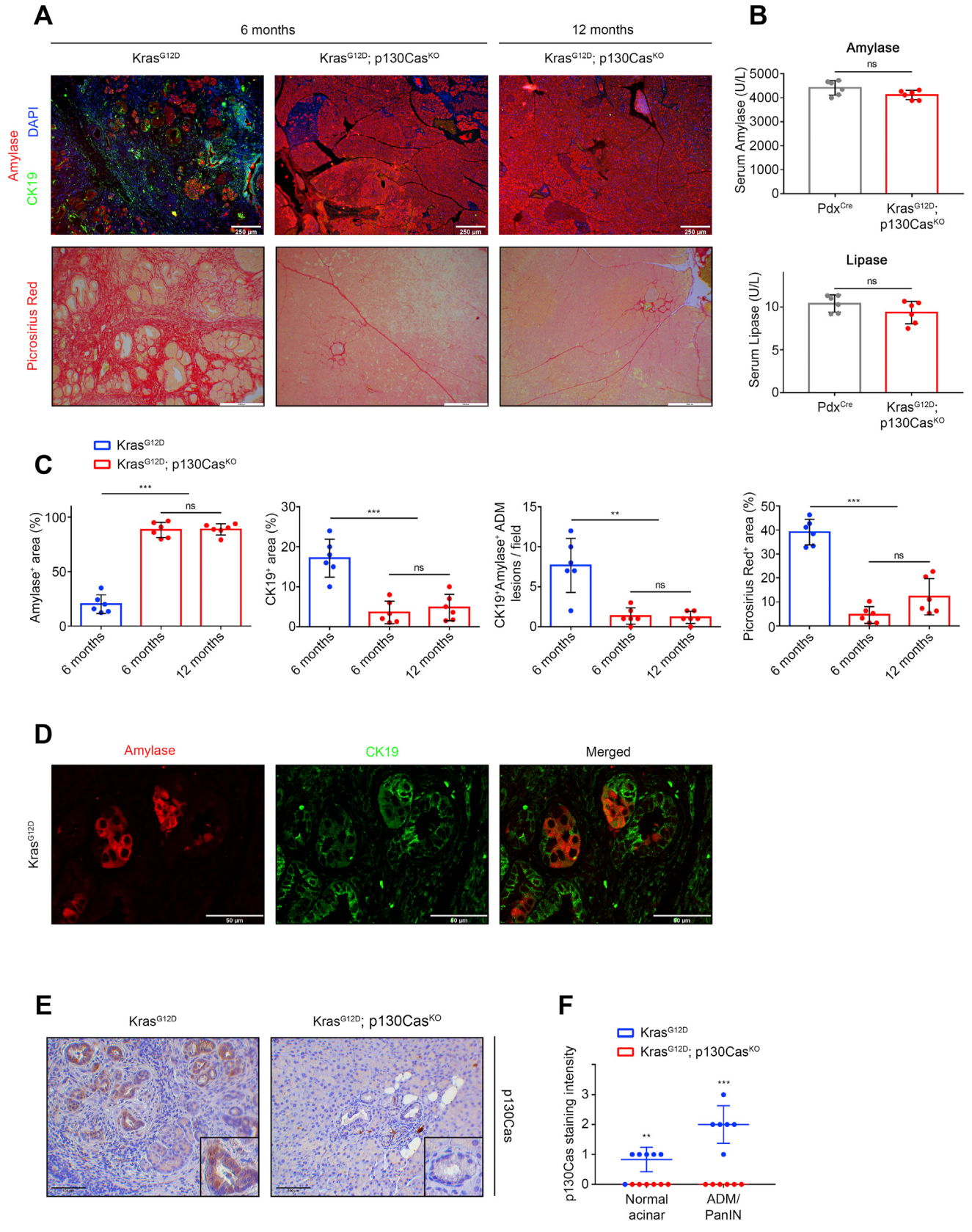
A
6 months
12 months
KrasG12D
KrasG12D; p130CasKO
KrasG12D
KrasG12D; p130CasKO
KrasG12D; p130CasKO
Amylase
CK19
DAPI
Picrosirius Red
250 μm
B
Amylase
ns
Serum Amylase (U/L)
5000
4000
3000
2000
1000
0
PdxCre
KrasG12D; p130CasKO
Lipase
ns
Serum Lipase (U/L)
10
5
0
PdxCre
KrasG12D; p130CasKO
C
KrasG12D
KrasG12D; p130CasKO
Amylase+ area (%)
CK19+ area (%)
CK19+Amylase+ ADM lesions / field
Picrosirius Red+ area (%)
***
**
ns
6 months
6 months
12 months
D
Amylase
CK19
Merged
KrasG12D
50 μm
80 μm
80 μm
E
KrasG12D
KrasG12D; p130CasKO
p130Cas
F
KrasG12D
KrasG12D; p130CasKO
p130Cas staining intensity
Normal acinar
ADM/ PanIN

Supplementary Figure 4. (*A*) Pancreatic tissue (normal acinar area and regions with ADM and PanINs) from $Kras^{G12D}$ and $Kras^{G12D}$; $p130Cas^{KO}$ mice was analyzed by immunofluorescence for expression of amylase (*red*), CK19 (*green*), and 4′,6-diamidino-2-phenylindole (DAPI) (*blue*), as indicated (*upper panel*). Collagen deposition and fibrosis was revealed with Picrosirius red staining (*lower panel*). (*B*) Circulating levels (U/L) of the pancreatic enzyme amylase and lipase in 12-month-old control Pdx^{Cre} and $Kras^{G12D}$; $p130Cas^{KO}$ mice. (*C*) Statistical analysis of amylase-positive, CK19-positive areas of pancreata from $Kras^{G12D}$ ($n = 6$) and $Kras^{G12D}$; $p130Cas^{KO}$ ($n = 6$) mice. Quantification and statistical analysis of $CK19^{+}/Amy^{+}$ double-positive ADM lesions. Statistical analysis of Picrosirius red–positive areas of pancreata from $Kras^{G12D}$ ($n = 6$) and $Kras^{G12D}$; $p130Cas^{KO}$ ($n = 6$) mice. (*D*) Representative examples of $CK19^{+}/Amy^{+}$ double-positive ADM lesions. (*E*) Immunohistochemistry for p130Cas in 4-month-old from $Kras^{G12D}$ and $Kras^{G12D}$; $p130Cas^{KO}$ pancreata showing absence of p130Cas expression in rare lesions present in KO animals. (*F*) Quantification of p130Cas immunohistochemical staining intensity, ranging from absent (0) to highest (3).

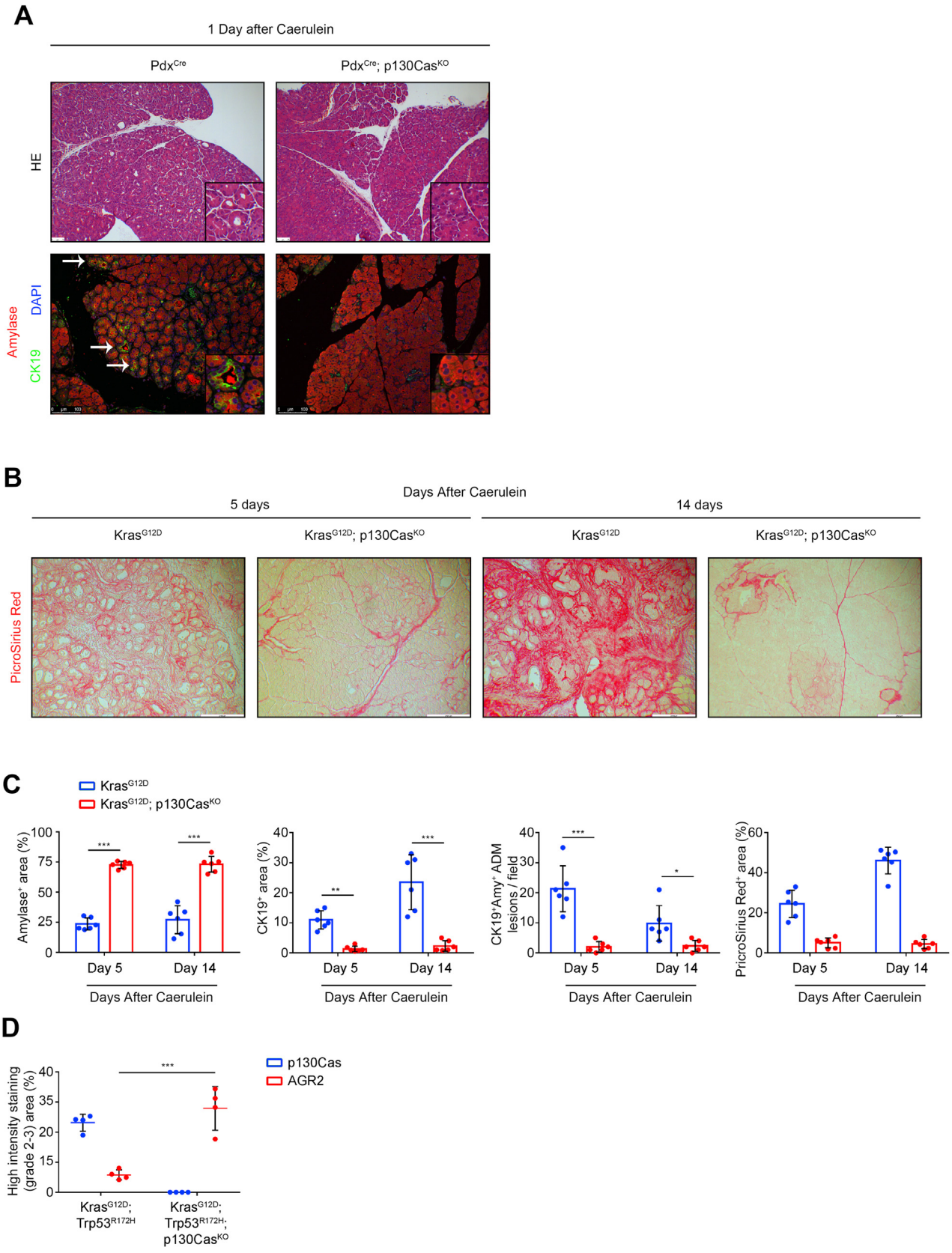
A
1 Day after Caerulein
PdxCre
PdxCre; p130CasKO
HE
Amylase
CK19
DAPI
B
Days After Caerulein
5 days
14 days
KrasG12D
KrasG12D; p130CasKO
PicroSirius Red
C
KrasG12D
KrasG12D; p130CasKO
Amylase+ area (%)
CK19+ area (%)
CK19+Amy+ ADM lesions / field
PricroSirius Red+ area (%)
Day 5
Day 14
Days After Caerulein
D
High intensity staining (grade 2-3) area (%)
p130Cas
AGR2
KrasG12D; Trp53R172H
KrasG12D; Trp53R172H; p130CasKO

Supplementary Figure 5. (*A*) Pancreatic tissue from Pdx^{Cre} and Pdx^{Cre}; $p130Cas^{KO}$ mice after caerulein treatment was stained with H&E or analyzed by immunofluorescence for expression of amylase (*red*), CK19 (*green*), and 4′,6-diamidino-2-phenylindole (DAPI) (*blue*), as indicated. (*B*) Pancreatic tissue (normal acinar area and regions with ADM and PanINs) from $Kras^{G12D}$ and $Kras^{G12D}$; $p130Cas^{KO}$ mice after caerulein treatment was analyzed for collagen deposition and fibrosis by Picrosirius red staining. (*C*) Statistical analysis of amylase-positive, CK19-positive areas of pancreata from $Kras^{G12D}$ ($n = 6$) and $Kras^{G12D}$; $p130Cas^{KO}$ ($n = 6$) mice after caerulein treatment. Quantification and statistical analysis of $CK19^{+}/Amy^{+}$ double-positive ADM lesions. Statistical analysis of Picrosirius red–positive areas of pancreata from $Kras^{G12D}$ ($n = 6$) and $Kras^{G12D}$; $p130Cas^{KO}$ ($n = 6$) mice after caerulein treatment. (*D*) Quantification of p130Cas and AGR2 immunohistochemical staining intensity, ranging from absent (0) to highest (3). Statistical analysis was performed with 2-way analysis of variance and presented as mean ± SD. ***$P < .001$.